Intercomparison of shortwave radiative transfer codes and measurements

Rangasayi N. Halthore,[1] David Crisp,[2] Stephen E. Schwartz,[3] G. P. Anderson,[4] A. Berk,[5] B. Bonnel,[6] O. Boucher,[6] Fu-Lung Chang,[7] Ming-Dah Chou,[8,9] Eugene E. Clothiaux,[10] P. Dubuisson,[11] Boris Fomin,[12] Y. Fouquart,[6] S. Freidenreich,[13] Catherine Gautier,[14] Seiji Kato,[15] Istvan Laszlo,[16] Z. Li,[7] J. H. Mather,[17] Artemio Plana-Fattori,[18] V. Ramaswamy,[13] P. Ricchiazzi,[14] Y. Shiren,[14] A. Trishchenko,[19] and W. Wiscombe[20]

Received 28 July 2004; revised 27 December 2004; accepted 23 February 2005; published 3 June 2005.

[1] Computation of components of shortwave (SW) or solar irradiance in the surface-atmospheric system forms the basis of intercomparison between 16 radiative transfer models of varying spectral resolution ranging from line-by-line models to broadband and general circulation models. In order of increasing complexity the components are: direct solar irradiance at the surface, diffuse irradiance at the surface, diffuse upward flux at the surface, and diffuse upward flux at the top of the atmosphere. These components allow computation of the atmospheric absorptance. Four cases are considered from pure molecular atmospheres to atmospheres with aerosols and atmosphere with a simple uniform cloud. The molecular and aerosol cases allow comparison of aerosol forcing calculation among models. A cloud-free case with measured atmospheric and aerosol properties and measured shortwave radiation components provides an absolute basis for evaluating the models. For the aerosol-free and cloud-free dry atmospheres, models agree to within 1% (root mean square deviation as a percentage of mean) in broadband direct solar irradiance at surface; the agreement is relatively poor at 5% for a humid atmosphere. A comparison of atmospheric absorptance, computed from components of SW radiation, shows that agreement among models is understandably much worse at 3% and 10% for dry and humid atmospheres, respectively. Inclusion of aerosols generally makes the agreement among models worse than when no aerosols are present, with some exceptions. Modeled diffuse surface irradiance is higher than measurements for all models for the same model inputs. Inclusion of an optically thick low-cloud in a tropical atmosphere, a stringent test for multiple scattering calculations, produces, in general, better agreement among models for a low solar zenith angle (SZA = 30°) than for a high SZA (75°). All models show about a 30% increase in broadband absorptance for 30° SZA relative to the clear-sky case and almost no enhancement in absorptance for a higher SZA of 75°, possibly due to water vapor line saturation in the atmosphere above the cloud.

Citation: Halthore, R. N., et al. (2005), Intercomparison of shortwave radiative transfer codes and measurements, *J. Geophys. Res.*, *110*, D11206, doi:10.1029/2004JD005293.

[1]Remote Sensing Division, Naval Research Laboratory, Washington, D. C., USA.
[2]NASA New Millennium Program, Jet Propulsion Laboratory, Pasadena, California, USA.
[3]Atmospheric Sciences Division, Brookhaven National Laboratory, Upton, New York, USA.
[4]Solar and Thermal Atmospheric Radiation, NOAA Climate Monitoring and Diagnostics Laboratory, Boulder, Colorado, USA.
[5]Spectral Sciences Inc., Burlington, Massachusetts, USA.
[6]Laboratoire d'Optique Atmospherique, Villeneuve d'Ascq, France.
[7]Earth System Science Interdisciplinary Center, University of Maryland at College Park, College Park, Maryland, USA.
[8]Laboratory for Atmospheres, NASA Goddard Space Flight Center, Greenbelt, Maryland, USA.
[9]Now at Department of Atmospheric Sciences, National Taiwan University, Taipei, Taiwan.
[10]Department of Meteorology, Pennsylvania State University, University Park, Pennsylvania, USA.
[11]ELICO, Université du Littoral Côte d'Opale, Wimereux, France.
[12]Kurchatov Institute, Moscow, Russia.
[13]NOAA Geophysical Fluid Dynamics Laboratory, Princeton University, Princeton, New Jersey, USA.
[14]Institute for Computational Earth System Science, University of California, Santa Barbara, California, USA.
[15]Center for Atmospheric Sciences, Hampton University, Hampton, Virginia, USA.
[16]NOAA National Environmental Satellite Data and Information Service, Camp Springs, Maryland, USA.
[17]Pacific Northwest National Laboratory, Richland, Washington, USA.
[18]Department of Atmospheric Sciences, Institute of Astronomy and Geophysics, University of Sao Paulo, Sao Paulo, Brazil.
[19]Canada Centre for Remote Sensing, Natural Resources Canada, Ottawa, Ontario, Canada.
[20]Climate and Radiation Branch, Laboratory for Atmospheres, NASA Goddard Space Flight Center, Greenbelt, Maryland, USA.

0148-0227/05/2004JD005293$09.00

1. Introduction

[2] Solar energy in the shortwave wavelength range spanning ~0.3 to 5 μm is the principal determinant of the atmospheric state. It is important to have a complete and accurate knowledge of the partitioning of this solar energy in the atmosphere into that absorbed, transmitted, and reflected to reliably estimate the response and evolution of the atmospheric state to various natural and anthropogenic perturbations. Although atmospheric molecules and aerosols scatter some of the incident solar energy back to space, thus providing a cooling effect, the same components absorb incident shortwave radiation to cause substantial heating of the atmosphere. However, the magnitude of the atmospheric shortwave absorption, approximately 20% absorptance according to past "textbook" estimates [e.g., *Peixoto and Oort*, 1992], appears to be highly uncertain; for example, an estimate using satellite data [*Li et al.*, 1997] yields a much higher 24% absorptance. Recent studies have shown considerable discrepancy between modeled and measured components of the atmospheric shortwave radiation in both cloudy and cloud-free skies, indicating that large uncertainties may be unaccounted for in measurements or that possible absorption mechanisms may be either underrepresented or perhaps completely absent in radiative transfer models. An object of this paper is to determine whether atmospheric absorption processes are accurately represented in radiative transfer models and to determine whether or not any of the models analyzed here exhibits a serious discrepancy.

[3] Using specified model inputs, here we compare the computation of the four atmospheric irradiance quantities in broadband and three wavelength intervals, ultraviolet (UV), visible (VIS), and infrared (IR), the direct solar irradiance at the surface, hereinafter sometimes referred to as the direct solar irradiance (whose monochromatic value at wavelength λ is designated by $E^{\downarrow}_{\lambda,dir}$), diffuse solar surface irradiance ($E^{\downarrow}_{\lambda,dif}$), upward shortwave flux at the surface ($E^{\uparrow}_{\lambda,S}$), and upward shortwave flux at the top of the atmosphere ($E^{\uparrow}_{\lambda,TOA}$). Heating rates are not considered. However, we also compare the computation of atmospheric absorption (as absorptance, A, the fraction of TOA irradiance that is absorbed in the atmosphere) which can be expressed as a function of the above four quantities. For example, absorptance in a given wavelength interval $\Delta\lambda$ (which would be one of the four wavelength intervals: UV, VIS, IR, and broadband) is calculated as

$$A_{\Delta\lambda} = \frac{\int_{\Delta\lambda} \left[\left(E^{\downarrow}_{\lambda,TOA} - E^{\uparrow}_{\lambda,TOA}\right) - \left(E^{\downarrow}_{\lambda,S} - E^{\uparrow}_{\lambda,S}\right)\right] d\lambda}{\int_{\Delta\lambda} E^{\downarrow}_{\lambda,TOA} d\lambda},$$

where $E^{\downarrow}_{\lambda,TOA}$ is the top-of-atmosphere (TOA) direct solar irradiance at wavelength λ and $E^{\downarrow}_{\lambda,S}$ is the total surface irradiance at $\lambda = E^{\downarrow}_{\lambda,dir} + E^{\downarrow}_{\lambda,dif}$.

[4] For the same inputs, models often disagree in the computed values of these irradiance quantities. For example, previous shortwave (SW) radiative transfer model intercomparison efforts have shown poor agreement among codes even for cases that involved only water vapor absorption. *Fouquart et al.* [1991] find substantial discrepancies among model results with standard deviation as a percentage of the mean (STDVM) ranging from 1% to 3% for the downward fluxes and 6–11% for the total atmospheric absorption, for a relatively simple case of pure water vapor absorption. That study was an important step in evaluating the agreement among the results of various shortwave radiative transfer codes for a common set of reference inputs. Considering that a 1% uncertainty in extraterrestrial solar irradiance or atmospheric absorptance can give rise to a ~1 K uncertainty in surface temperature (calculated for an idealized case by applying shortwave radiative balance to Earth as a spherical planet with uniform surface properties and whose period of rotation is short when compared with the atmospheric radiative time constant), it is important that the model results agree to a much better degree if they are to be useful in climate modeling.

[5] Since the *Fouquart et al.* [1991] study, radiative transfer models have undergone a number of improvements ranging from better characterization and representation of atmospheric state in models to more accurate representation and calculation of radiative transfer. Thus, to check the current status of model agreements in computation of important atmospheric properties, we have undertaken a study of 16 commonly used radiative transfer models ranging in wavelength resolution from line-by-line models to broadband models (Table 1). The study was an outgrowth of discussions held at the Gordon Conference on Solar Radiation and Climate in June 1998 in Plymouth, New Hampshire (http://www.grc.uri.edu/programs/1998/solarad.htm). Participants agreed to perform model intercomparisons for cloud-free and cloudy atmospheres to compare models against each other and where possible, to evaluate the models against measurements. Model-to-model intercomparisons have value as not all models are equal: Some, such as the line-by-line models, treat transmittance more explicitly, whereas some broadband models use more approximate methods that provide the speed needed in climate simulations. With the increase in computation power, models are becoming quite comprehensive in their treatment of radiative transfer by including computationally intensive multiple scattering schemes along with detailed representation of line-by-line molecular absorption and continuum absorption of all the important atmospheric species. Model-to-measurement comparisons provide a reality check if the accuracy of the measurements is known. Most participants agreed to bring the models they either developed or routinely use to this intercomparison effort (Table 1; see Appendix A for a brief description of each model). *Barker et al.* [2003] performed an intercomparison study involving various one-dimensional (1-D) and three-dimensional (3-D) radiative transfer codes with emphasis on cloud interactions with shortwave radiation. Where appropriate, we discuss and compare the findings of that study to those of the present study.

1.1. Protocol

[6] For each case listed below, the atmospheric radiation components that were calculated and reported are, in order of increasing complexity, $E^{\downarrow}_{dir}$, $E^{\downarrow}_{dif}$, $E^{\uparrow}_{S}$, and $E^{\uparrow}_{TOA}$, where the subscript λ is omitted with the understanding that these components are calculated for four wavelength intervals:

Table 1. Models, Model Characteristics and Investigators

Model Number	Description of Models[a]	Investigator(s)
1	ATRAD2; doubling-adding (D-A) model; LOWTRAN 7 transmittance; 193 spectral intervals between 200 and 4000 nm	Laszlo, Wiscombe
2	D-A model; Modtran 3.5 atmospheric transmittance; 105 unequal spectral intervals within 0.2–5 μm; 11 streams in each hemisphere	Li, Trishchenko
3	D-A model; correlated-K method for H_2O transmittance and LOWTRAN-7 for other gases; 120 wavelength bands; eight vertical layers	Chang
4	GAME; Discrete Ordinate Method; correlated k-distribution method for H_2O and CO_2 transmittance; spectral resolution: 10 cm^{-1} from 0.2 to 5 μm; 33 vertical layers	Bonnel, Boucher, Dubuisson, Fouquart
5	GAME: same as Model 4 but with a spectral resolution of 100 cm^{-1} (from 0.5 to 5 μm) or 400 cm^{-1} (from 0.2 to 0.5 μm)	Bonnel, Boucher, Dubuisson, Fouquart
6	SBDART; 20 cm^{-1} spectral resolution; 1 km vertical resolution in troposphere; 33 altitude layers	Gautier, Ricchiazzi, Shiren
7	SBMOD; 1-nm resolution; uses k-distribution look-up table based on HITRAN; same cloud, aerosol, and surface models as SBDART	Gautier, Ricchiazzi, Shiren
8	RAPRAD, delta-four-stream approximation	Clothiaux, Kato, Mather
9	Discrete Ordinate Method (DISORT); LBL	Chou
10	D-A model; LBL	Freidenrich, Ramaswamy
11	GAME: Discrete Ordinate Method; line-by-line calculations for gaseous absorption; high spectral resolution (<0.01 cm^{-1}); 33 vertical layers	Bonnel, Boucher Dubuisson, Fouquart
12	DISORT; LBL	Crisp
13	Monte Carlo; LBL	Fomin, Plana-Fattori
14	MODTRAN-4; 2-stream Isaacs' model; HITRAN based transmittance; 2 cm^{-1} wavelength resolution; 50 vertical layers	Anderson, Berk, Halthore, Schwartz
15	MODTRAN-4; eight-stream DISORT model; HITRAN based transmittance; 2 cm^{-1} wavelength resolution; 50 vertical layers	Anderson, Berk, Halthore, Schwartz
16	GCM	Chou

[a]For details, see Appendix A. Entries are arranged as follows: name, if any; multiple scattering scheme; gaseous transmittance; wavelength resolution; vertical resolution.

broadband shortwave (0.28–5.0 μm), ultraviolet (UV, 0.2–0.35 μm), visible (VIS, 0.35–0.7 μm), and shortwave infrared (SWIR, 0.7–5.0 μm). Of these components, the direct solar irradiance at the surface, $E^{\downarrow}_{dir}$, is the simplest since it depends only on the knowledge of the wavelength-dependent extraterrestrial solar flux and the atmospheric extinction, without regard to details of extinction, namely absorption or scattering. Furthermore, $E^{\downarrow}_{dir}$ can be most accurately measured with the aid of absolute irradiance measuring devices such as an active cavity radiometer (with an accuracy of ~2 W m^{-2} in a measurement of ~1000 W m^{-2}). Diffuse downward irradiance at the surface, $E^{\downarrow}_{dif}$, depends on the multiply scattered solar energy in the atmosphere by molecules, aerosols, and clouds directed toward the surface. This in turn depends on the size and refractive index of particles doing the scattering. A small but non-negligible contribution to this quantity is due to multiple reflections of light between the atmosphere and the surface. The upward flux at the surface, $E^{\uparrow}_{S}$, depends on the total energy falling on the surface (both direct and diffuse) and on the bidirectional surface reflectance characteristics. For the surface albedo, or reflectance, that is constant with respect to wavelength, the upward flux at the surface is just the albedo, or reflectance, multiplied by the total downward irradiance. The protocol, input data, and results for individual models are provided at the internet web site, hereinafter called the Project Web Site[1].

[1]Auxiliary material is available at ftp://ftp.agu.org/apend/jd/2004JD005293.

1.2. Cases to Be Treated

1.2.1. Case I: Rayleigh Scattering Atmosphere

[7] Shortwave irradiance components were computed for two standard atmospheres [*Anderson et al.*, 1986], the subarctic winter (SAW, low humidity) and tropical atmosphere (TROP, high humidity), and at two solar zenith angles (SZA), 30° and 75°, that provide a range of conditions. A wavelength-independent Lambertian surface albedo of 0.2 in the wavelength range 0.28 to 5.0 μm was to be used along with a solar spectrum taken from MODTRAN (Model 15, Table 1) commonly referred to as the Kurucz spectrum [*Kurucz*, 1994; *Berk et al.*, 1998]. In addition to N_2 and O_2, specified also are minor gas (i.e., H_2O, O_3) abundances as a function of height from MODTRAN with a mixing ratio of 360 ppm (μmol mol^{-1}, of dry air) for CO_2. Calculations are reported for the four wavelength intervals. Vertical resolution was not specified; it was left to the participating groups to follow their usual practice. This aerosol-free case highlights the transmittance part of the codes, with the line-by-lines providing the benchmarks for the direct irradiance.

1.2.2. Case II: Atmosphere With Aerosols

[8] The model atmospheres for Case I are augmented with two aerosol loadings: high aerosol optical thickness or "high AOT" (AOT = 0.24 at 550 nm; Ångström exponent $b \equiv -d\log \tau_a/d\lambda = 1.6$) and "low AOT" (0.08; b = 0.74). Aerosol scattering properties, single scattering albedo (SSA), asymmetry parameter, and phase function are calculated from Mie theory as a function of wavelength for specified aerosol lognormal size distribution with the following properties: a geometric mean radius of 0.027 μm and a standard deviation of 0.77 μm which pertain to the accumulation mode "urban average" aerosols described by

Whitby [1978]; refractive indices (1.42−0.0079*i*) for size limits 0.0 to 10 μm. Investigators were asked to interpolate as needed. Clearly, in this approach the aerosol properties are overspecified, as the optical thickness and Ångström exponent are dependent on size distribution and refractive index. This case highlights the accuracy of models in handling multiple scattering.

1.2.3. Aerosol Forcing

[9] Cases I and II provide the information necessary to calculate aerosol forcing for particular components of radiation. Forcing for a component is defined as the difference in flux value with and without aerosols present in the atmosphere. Without aerosol scattering and absorption, the atmosphere will still have molecular (Rayleigh) scattering and molecular absorption. For an outgoing component, such as upward TOA flux, positive values of forcing imply cooling by aerosols since more energy is leaving the atmosphere with aerosols present than without. Here aerosol forcing is calculated for three components: TOA upward flux, surface upward flux, and surface downward flux for the two atmospheres (SAW and TROP), for the two aerosol loadings and the two solar zenith angles. Aerosol forcing is a sensitive measure of model treatment of the aerosol, as the subtraction of the flux components leads, to first order, to cancellation of errors in treatment of the aerosol-free atmosphere. Consequently, differences in aerosol forcing will represent primarily differences in treatment of the aerosol by the model, or differences in the properties of the aerosol represented in the model. Aerosol forcing is of considerable current interest in the context of anthropogenic climate change, having been identified by the *Intergovernmental Panel on Climate Change* [2001] as a major source of uncertainty in radiative forcing of climate change over the industrial period.

1.2.4. Case III: Two Observed Cases

[10] Code comparisons are performed for two cases for which measurements of direct and diffuse solar irradiance measurements are available; these cases are distinguished by the value of AOT at 550 nm, 0.24 and 0.08 corresponding to cases 37 and 13, respectively, in Table 1, *Halthore and Schwartz* [2000]. Specified also are atmospheric lapse rates, solar zenith angles (51.39° and 27.08°, respectively), Angstrom exponents (1.6 and 0.74), single scattering albedo (0.88 and 0.94), asymmetry parameter (0.7 and 0.6), precipitable water (3.26 and 1.11 cm), and surface reflectance, obtained from measurements in most cases. The direct irradiance measurement (436 and 862 W m^{-2}) was obtained from a normal incidence pyrheliometer which is ultimately calibrated against absolute cavity radiometers, and the diffuse irradiance measurement (141 and 89 W m^{-2}) is obtained from Eppley laboratory's precision spectral pyranometer (ventilated) with appropriate corrections for zero offsets as described by *Halthore et al.* [1998] and *Halthore and Schwartz* [2000]. This case represents a reality check for all models. Some components of the atmospheric radiation field such as the direct solar irradiance can be measured accurately, while others, such as the diffuse downward irradiance, have larger errors.

1.2.5. Case IV: Atmosphere With Cloud

[11] This case consists of a cloudy layer located between 1 and 2 km (904 and 805 mbar) in an aerosol-free tropical model atmosphere (same as in Case I) with an integrated optical depth of 60 at 550 nm [*Dong et al.*, 1997]. This corresponds to a uniform mixing ratio of about 146 particles/cm^3. The wavelength-dependent optical properties are defined corresponding to a lognormal size distribution with a modal radius of 7 μm and a logarithmic width of 0.35. Refractive index values are from *Ray* [1972] and *Segelstein* [1981]. Broadband modelers were requested to use their own method of creating broadband results from high wavelength resolution data. Provided also was the cloud particle phase function tabulated at 181 angles at each of the 188 wavelengths (0.2 to 8.1 μm) together with the Legendre polynomial moments. The surface albedo is assumed to be 0.2 (independent of wavelength).

2. Results

[12] The results for each case are tabulated as average values and as standard deviations as a percentage of the mean (STDVM) to enable evaluation of overall model agreement. In specific cases where the agreement is particularly poor, results are plotted to identify the source of the discrepancy.

2.1. Results for Case 1

[13] Results for Case 1 (Rayleigh atmosphere), summarized in Table 2, show that in the computation of the broadband direct solar irradiance the models agree best, as indicated (columns 6–9) by a low value of the STDVM when slant-path water vapor is lowest (STDVM ∼0.5, 30° SZA, SAW case), and worst when it is highest (STDVM ∼1.9, 75° SZA, TROP case). This level of agreement to within a few percent STDVM (Table 2 and Figure 1a) is a result of models using similar gaseous absorption databases. Agreement is poorer in the UV range (Table 2, Figure 1b), probably because some models ignore gaseous absorption in view of the relatively small amount of solar energy in this range and/or use data from different sources (see Appendix A). Another possibility is that the models compute absorptance along optical paths that may or may not be corrected for spherical geometry and/or refractive effects. The consequences for the integrated flux are negligible because of the small magnitude of the energy in this range. Nevertheless, direct solar irradiance in the UV as calculated by the different models (Figure 1b) shows that models 4, 5, 8, and 9 calculate slightly higher values (by ∼1 Wm^{-2}) than the rest, indicating that they may have underestimated the absorption. This trend is seen whether or not aerosols are present (see also Case 2 discussion below).

[14] In the visible range, where gaseous absorption is low, model agreement for $E^{\downarrow}_{dir}$ is predictably good (0.37% and 1.9% STDVM, 30° and 75° SZA, respectively (Table 2)) for both the SAW and TROP atmospheres, indicating that water vapor absorption is small and is correctly parameterized. The parameterization of water vapor absorption was of concern since the band strengths used in many of the radiative transfer (RT) models were based on erroneous line strengths tabulated in the HITRAN database [*Giver et al.*, 2000]; at the time of this study, only MODTRAN-4 had corrected water vapor absorption coefficients. The degree of agreement among the models, as indicated by the STDVM, with and without the MODTRAN-4 models, does not appear to be affected (result not shown), indicating that

Table 2. Case 1, Computations for a Rayleigh Atmosphere[a]

	Average, Irradiance in W m^{-2}				Standard Deviation as a % of Mean			
	Subarctic Winter		Tropical		Subarctic Winter		Tropical	
	30.00° SZA	75.00° SZA	30.00° SZA	75.00° SZA	30.00° SZA	75.00° SZA	30.00° SZA	75.00° SZA
				Direct Down				
0.28–5.00 μm	940.9	217.0	848.5	184.8	0.54	1.46	0.68	1.89
0.20–0.35 μm	11.5	0.4	11.8	0.4	3.01	8.89	3.22	8.88
0.35–0.70 μm	414.0	81.4	413.3	81.3	0.37	1.90	0.37	1.90
0.70–5.00 μm	515.3	135.2	423.4	103.0	0.95	1.52	1.31	2.35
				Diffuse Down				
0.28–5.00 μm	63.8	37.1	64.0	37.2	2.34	1.30	2.18	3.91
0.20–0.35 μm	9.0	2.8	9.5	3.0	3.03	3.41	2.83	3.44
0.35–0.70 μm	50.3	30.7	50.3	30.9	2.59	1.20	2.52	1.23
0.70–5.00 μm	4.4	3.5	4.2	3.4	3.15	5.71	31.36	39.81
				Diffuse Up				
0.28–5.00 μm	201.1	50.9	183.1	45.0	0.48	1.45	1.06	4.49
0.20–0.35 μm	4.1	0.6	4.3	0.7	2.54	4.65	2.62	4.29
0.35–0.70 μm	92.9	22.4	92.7	22.4	0.41	1.61	0.40	1.61
0.70–5.00 μm	104.0	27.8	86.2	21.9	0.91	1.64	2.25	8.57
				Diffuse Up TOA				
0.28–5.00 μm	227.4	82.3	207.0	76.2	1.41	1.27	1.83	1.52
0.20–0.35 μm	9.7	4.0	10.2	4.1	5.27	4.39	4.59	4.06
0.35–0.70 μm	118.9	48.8	119.2	49.3	1.52	1.50	1.51	1.52
0.70–5.00 μm	98.8	29.5	77.6	22.8	2.01	1.98	3.04	4.62
				Absorptance				
0.28–5.00 μm	0.125	0.189	0.205	0.281	3.87	4.76	2.33	3.26
0.20–0.35 μm	0.472	0.555	0.449	0.536	3.42	2.94	3.37	3.00
0.35–0.70 μm	0.033	0.086	0.033	0.082	12.40	13.83	12.30	14.75
0.70–5.00 μm	0.180	0.252	0.332	0.428	4.77	4.38	2.64	2.68

[a]In this and all subsequent tables, "Direct Down" refers to symbol $E^{\downarrow}_{dir}$, "Diffuse Down" refers to $E^{\downarrow}_{dif}$, "Diffuse Up" refers to $E^{\uparrow}_{S}$, "Diffuse Up TOA" refers to $E^{\uparrow}_{TOA}$, and "Absorptance" refers to, A. SZA denotes solar zenith angle.

the water vapor absorption coefficient corrections do not significantly affect wavelength-integrated fluxes. In the *Barker et al.* [2003] study, for the cloud-free sky case, several models using older spectroscopic databases underestimated the diurnal mean atmospheric absorption of solar radiation by 18 W m^{-2}, corresponding to an absorptance of 0.03, when compared to "benchmark" models that used parameterizations based on newer databases. This level of disagreement, about 3 times that found in our study, was tentatively attributed to lack of inclusion, or improper representation, of band and continuum absorption by water vapor.

[15] Downwelling broadband direct irradiance at the surface, $E^{\downarrow}_{dir}$, plotted in Figure 1c for the two atmospheres and two solar zenith angles as percent deviation from mean, shows that Model 5 (GAME model), with a wave number resolution of 100 cm^{-1}, has the greatest deviation; this model was excluded from calculations in other cases. In contrast, medium resolution models, such as Model 4 (GAME, 10 cm^{-1}) or MODTRAN (Model 15, 2 cm^{-1} resolution), appear to be adequate in computing gaseous absorption. This finding suggests that very high line-by-line resolution models may not be necessary for broadband computations of atmospheric absorptance.

[16] Departures from the means of several flux quantities for the SAW Rayleigh case (and SZA = 30°) are shown in Figure 1d in W m^{-2}. For most of the models, positive deviation of direct downwelling flux at the surface, $E^{\downarrow}_{dir}$, is correlated with and comparable to negative of atmospheric absorption with model 14 (which uses two-stream approx-

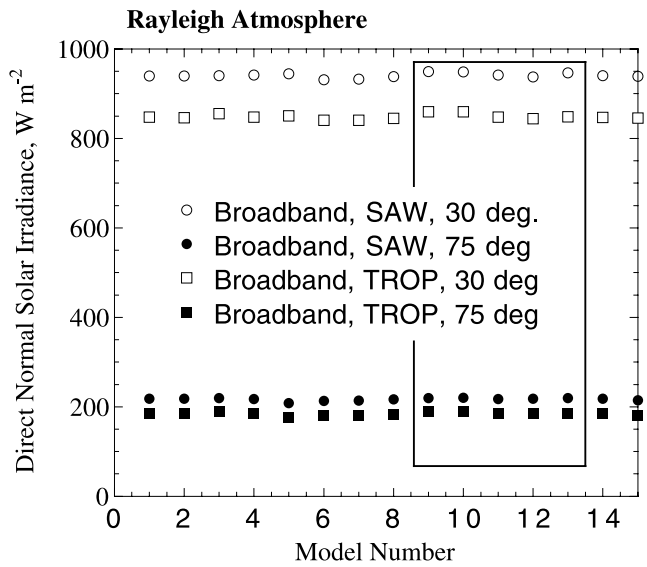

Figure 1a. Broadband direct-normal solar irradiance plotted for the atmospheric and geometric conditions as a function of model number for Case 1 (Rayleigh atmosphere) shows excellent agreement among models, confirming that the gaseous absorption in the models is also in agreement. Average values and STDVMs for this case are given in Table 2. Models 9 through 13 enclosed in the shaded rectangle are line-by-line models and are identified thus in some of the following figures.

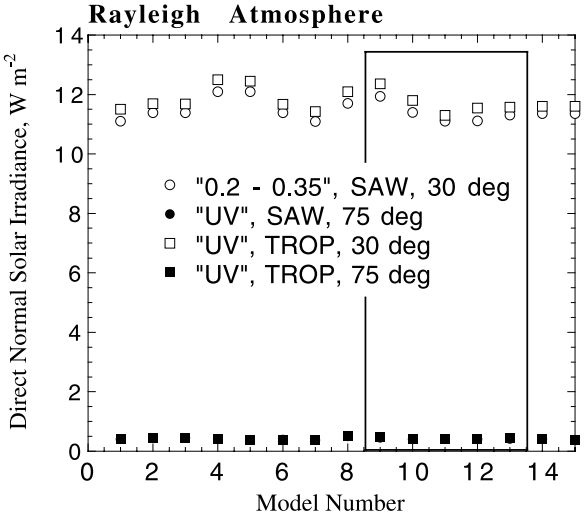

Figure 1b. For Case 1, direct-normal solar irradiance in the UV (0.2–0.35 μm) is plotted similar to that in Figure 1a to show the variability that is encountered in this wavelength range. Consequences for the integrated flux are negligible because of the small magnitude of the energy in this range. The solid symbols for the two atmospheres and 75° SZA fully overlap.

imation to provide the necessary speed, not accuracy) being an outlier. This is because, in the absence of aerosols, the main reason for the differences in $E^{\downarrow}_{dir}$ is the differences in treatment of atmospheric gaseous absorption. For most of the models the absorption at the surface is correlated with, and comparable to, the negative of the absorption in the atmosphere, with model 14 again being an outlier (R^2 = 0.66 with model 14, 0.88 without). This is perhaps not surprising, as most of the energy incident at the surface is in the primary beam, so a decrease in incident flux will result in a decrease in surface absorbed flux. Without model 14, the spread of the data for diffuse upwelling flux at the TOA, or equivalently total absorption by the Earth-atmosphere system, exhibits about one half the spread of the atmospheric absorption (standard deviation 2.5 W m^{-2} compared with 5.8 W m^{-2}), indicating that the apparent good agreement in diffuse upwelling flux at the TOA is due in considerable part to compensating errors in the atmospheric and surface absorption.

2.2. Results for Case 2 (With Aerosols)

[17] Results for Case 2 (with aerosols), summarized in Tables 3a and 3b, show that the best agreement among the models for the low AOT case (Table 3a) is obtained for total downward irradiance and upward flux at the surface in the broadband for the SAW atmosphere (Figure 2a) and the total downward irradiance at the surface for the TROP atmosphere. The worst agreement for the low AOT case is in the computation of absorptance for the SAW atmosphere (Figure 2b) and diffuse downward flux at the surface for the TROP atmosphere. For both atmospheres, the agreement in the computation of total irradiance at the surface is better than for its components of direct and diffuse irradiance because of the conservative nature of scattering for which photons not directly transmitted predominantly manifest as diffuse light (absorption being the other mechanism) so that the total irradiance remains approximately the same. Clearly, compared with values for the SAW atmosphere, differences in the parameterization of water vapor absorption for the TROP atmosphere account for the larger model disagreements among all components, except the absorptance (columns 8–9 compared with columns 6–7, Table 3a). For the absorptance, the standard deviation among models increases more as a function of SZA than water vapor absorption and therefore is seen to be relatively insensitive to the type of atmosphere present. For high AOT, the best agreement among models is in the computation of diffuse surface irradiance (Figure 2c) and the worst, absorptance (Figure 2d). An improvement in agreement among models for the computation of absorptance is obtained for the 75° SZA, TROP case by excluding the GCM, model 16 (from 3.4% to 2.7%, column 9, Table 3b), which appears to be an outlier; still, it is reassuring that the performance of the GCM is as good as it is.

[18] One would expect that inclusion of aerosols in models with the attendant increase in uncertainties in specifying aerosol properties should increase the STDVM among models for most, if not all, of the irradiance quantities. However, we do not find this to be the case for all the irradiance quantities. Generally, 42 quantities out of 80 in Table 3a (Low AOT, columns 6–9) and 36 out of 80 in Table 3b (High AOT, columns 6–9) have a better agreement among models than for the aerosol-free case (Table 2, columns 6–9). Also, 27 quantities out of 80 in Table 3b (High AOT) have better agreement than in Table 3a (Low AOT). One possible explanation is that inclusion of aerosols in the atmospheres of the type used here decreases the fractional solar energy that is interacting with the constituents of the lower atmosphere with their associated uncertainties (such as uncertainties in aerosol and molecular optical properties), thus increasing the level

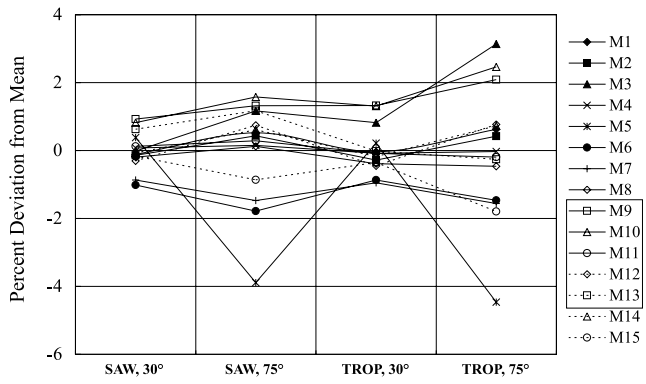

Figure 1c. For Case 1, broadband direct solar irradiance at the surface is plotted for the different models as percent deviation from mean for the two atmospheres and two SZAs. Model 5 (GAME model with a wave number resolution of 100 cm^{-1}) shows the most deviation and was subsequently discontinued from calculations in other cases. The results from GCM (Model 16) are not included here because the model does not calculate the direct and diffuse components of the global irradiance separately. Line-by-line models are identified by the box in the legend description.

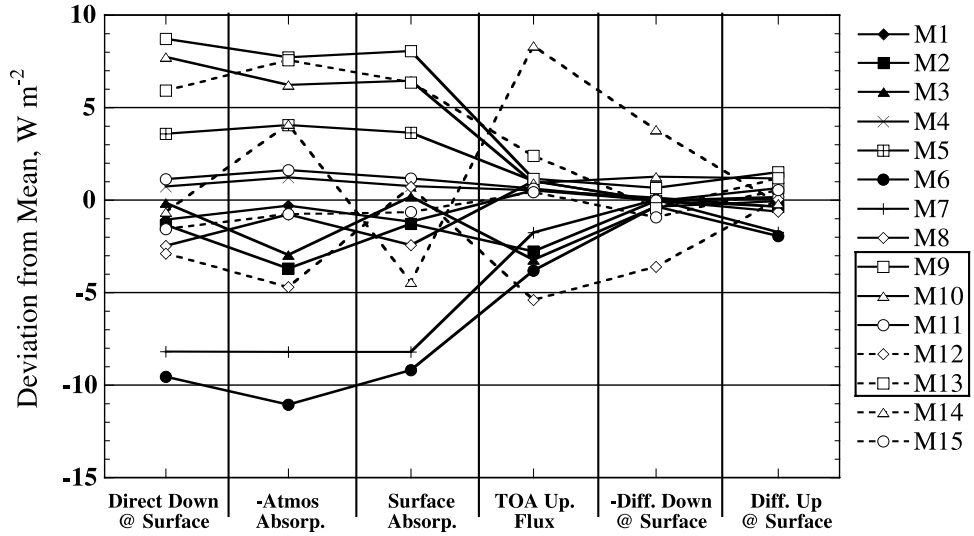

Figure 1d. For Case 1 SAW atmosphere, SZA = 30°, comparison among the 15 models is shown for six flux quantities as deviation from the mean in W m^{-2}. The components are direct irradiance at the surface, negative of atmospheric absorption, absorption at the surface, diffuse upwelling flux at the TOA, negative of diffuse irradiance at the surface, and diffuse upwelling flux at the surface. The mean quantities respectively are, in W m^{-2}, 940.91, 147.03, 803.66, 227.40, 63.80, and 201.05.

Table 3a. Case 2, Computations With Aerosols, Low AOT[a]

	Average, Irradiance in W m^{-2}				Standard Deviation as a % of Mean			
	Subarctic Winter		Tropical		Subarctic Winter		Tropical	
	30.00° SZA	75.00° SZA	30.00° SZA	75.00° SZA	30.00° SZA	75.00° SZA	30.00° SZA	75.00° SZA
				Direct Down				
0.28–5.00 μm	872.07	171.67	784.22	144.76	0.65	1.62	0.76	2.12
0.20–0.35 μm	10.00	0.27	10.29	0.27	2.91	11.95	2.95	12.21
0.35–0.70 μm	376.08	59.80	375.37	59.72	0.27	1.29	0.30	1.42
0.70–5.00 μm	485.84	111.58	398.82	84.76	1.03	1.95	1.45	2.80
				Diffuse Down				
0.28–5.00 μm	120.12	64.53	116.51	61.95	2.10	1.84	2.86	3.34
0.20–0.35 μm	9.96	2.80	10.46	2.95	2.27	3.70	2.29	4.05
0.35–0.70 μm	82.29	43.91	82.19	44.09	1.63	0.97	1.58	0.96
0.70–5.00 μm	27.88	17.84	23.84	14.91	5.50	5.67	10.69	13.57
				Total Down				
0.28–5.00 μm	992.19	236.20	900.73	206.71	0.50	0.93	0.50	1.02
0.20–0.35 μm	19.96	3.07	20.76	3.22	2.16	3.81	2.18	4.29
0.35–0.70 μm	458.38	103.71	457.56	103.80	0.38	0.80	0.38	0.90
0.70–5.00 μm	513.73	129.42	422.65	99.67	0.88	1.35	1.16	1.92
				Diffuse Up				
0.28–5.00 μm	198.61	47.41	181.22	42.36	0.45	0.72	1.12	4.79
0.20–0.35 μm	3.99	0.61	4.15	0.64	2.05	5.24	2.28	5.51
0.35–0.70 μm	91.68	20.74	91.51	20.76	0.36	0.83	0.38	0.90
0.70–5.00 μm	102.91	26.05	85.55	20.95	0.79	1.25	2.39	10.22
				Diffuse Up TOA				
0.28–5.00 μm	228.46	91.82	208.53	85.54	1.57	1.30	2.00	2.20
0.20–0.35 μm	9.66	4.00	10.16	4.17	5.07	4.31	4.53	4.08
0.35–0.70 μm	119.72	52.99	120.03	53.62	1.61	1.22	1.57	1.16
0.70–5.00 μm	99.08	34.83	78.33	27.76	2.15	2.59	3.45	6.39
				Absorptance				
0.28–5.00 μm	0.132	0.203	0.212	0.290	3.67	3.05	2.15	2.22
0.20–0.35 μm	0.481	0.562	0.458	0.543	2.96	2.90	2.84	3.11
0.35–0.70 μm	0.041	0.103	0.041	0.098	8.69	5.49	8.37	5.96
0.70–5.00 μm	0.187	0.263	0.338	0.432	4.37	4.02	2.60	2.84

[a]In this and all subsequent tables, "Total Down" refers to symbol, $E_S^{\downarrow}$.

Table 3b. Case 2, Computations With Aerosols, High AOT

	Average, Irradiance in W m^{-2}				Standard Deviation as a % of Mean			
	Subarctic Winter		Tropical		Subarctic Winter		Tropical	
	30.00° SZA	75.00° SZA	30.00° SZA	75.00° SZA	30.00° SZA	75.00° SZA	30.00° SZA	75.00° SZA
				Direct Down				
0.28–5.00 μm	778.04	129.29	693.10	105.26	0.55	1.28	0.73	1.96
0.20–0.35 μm	6.29	0.14	6.46	0.14	6.90	123.57	6.86	121.46
0.35–0.70 μm	307.16	32.72	306.51	32.62	0.52	1.57	0.50	1.59
0.70–5.00 μm	464.48	96.48	380.09	72.57	0.96	1.57	1.38	2.58
				Diffuse Down				
0.28–5.00 μm	193.23	86.43	187.06	82.26	1.65	1.36	1.24	1.24
0.20–0.35 μm	12.12	2.60	12.67	2.75	2.95	5.57	2.85	5.75
0.35–0.70 μm	136.02	57.24	135.75	57.46	2.11	2.03	2.10	2.13
0.70–5.00 μm	45.10	26.59	38.64	22.06	1.16	1.79	3.82	6.51
				Total Down				
0.28–5.00 μm	971.27	215.72	880.17	187.52	0.52	0.95	0.57	0.99
0.20–0.35 μm	18.41	2.74	19.12	2.89	2.64	5.55	2.54	4.96
0.35–0.70 μm	443.18	89.96	442.26	90.08	0.45	1.18	0.46	1.29
0.70–5.00 μm	509.58	123.06	418.72	94.63	0.87	1.34	1.15	2.08
				Diffuse Up				
0.28–5.00 μm	194.42	43.31	177.05	38.52	0.43	0.74	1.04	5.22
0.20–0.35 μm	3.67	0.53	3.82	0.55	2.64	6.97	2.39	7.27
0.35–0.70 μm	88.64	17.99	88.45	18.01	0.44	1.22	0.45	1.30
0.70–5.00 μm	102.08	24.79	84.76	19.94	0.78	1.56	2.44	10.93
				Diffuse Up TOA				
0.28–5.00 μm	231.12	100.73	211.30	94.18	1.56	1.44	1.87	1.58
0.20–0.35 μm	9.79	4.07	10.30	4.23	5.15	4.73	4.67	4.41
0.35–0.70 μm	121.79	58.65	122.18	59.45	1.67	1.24	1.63	1.17
0.70–5.00 μm	99.54	38.01	78.82	30.51	2.15	3.21	3.36	5.33
				Absorptance				
0.28–5.00 μm	0.144	0.224	0.224	0.309	3.33	3.53	2.19	2.77
0.20–0.35 μm	0.503	0.574	0.482	0.555	2.92	3.54	2.82	3.43
0.35–0.70 μm	0.061	0.138	0.061	0.132	5.23	6.60	5.36	7.30
0.70–5.00 μm	0.192	0.273	0.342	0.439	4.26	4.25	2.56	3.30

of agreement among the models. Supporting this argument is that for all cases, total irradiance at the surface decreases slightly with increasing AOT.

[19] For low AOT, a SAW atmosphere, and a 30° SZA, the agreement is marginally better for the broadband diffuse irradiance ($E^{\downarrow}_{dif}$) than for the molecular case (2.1% versus 2.34%, Table 3a and Table 2, column 6). Of the 80 irradiance quantities (not including "Total Down" or $E^{\downarrow}_{S}$) in Table 3a, in a majority of cases, 45 out of 80, agreement among models is better than for the Rayleigh case (Table 2). Some of the other notable quantities for which agreement is better in the low AOT case than the Rayleigh case are: broadband absorptance, broadband $E^{\uparrow}_{dif,S}$ for SAW atmosphere, both SZAs, and surprisingly, all absorptance quantities except two (of 16).

[20] For the high AOT case (Table 3b), the STDVM among the models is predictably higher than that for the low AOT case for most components (48 components out of 80). This result, when considered with the better level of agreement for the low AOT case relative to a purely Rayleigh atmosphere, means that there is less uniformity in treating aerosol extinction in the models although there are exceptions for specific components of radiation. For example, for the 30°-SZA TROP atmosphere case (Table 3b, column 8) all the computed broadband shortwave irradiance/flux components except the absorptance and total downward

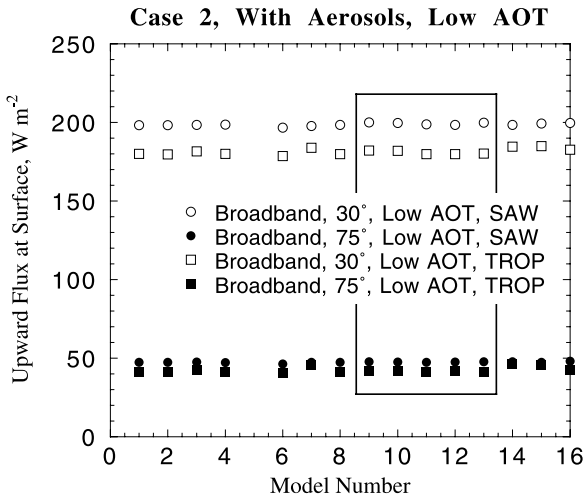

Figure 2a. For Case 2, with aerosols of low optical thickness, best agreement among models was obtained for the broadband upward flux at the surface. The STDVM for the four cases shown here are 0.43, 0.72, 1.12, and 4.79 for the 30° SAW, 75° SAW, 30° TROP, and 75° TROP cases, respectively.

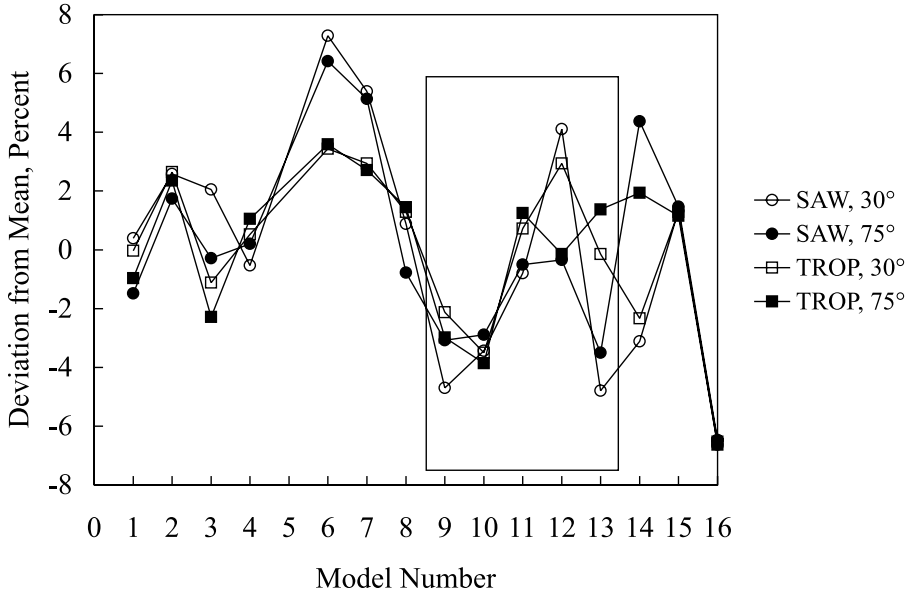

Figure 2b. Broadband absorptance is plotted as percent deviation from mean for the various models for atmospheres with aerosol included (Low AOT). The agreement for the absorptance seen here in Case 2 is among the worst for all components. The mean values are: 0.132 (SAW 30°), 0.202 (SAW 75°), 0.211 (TROP 30°), and 0.289 (TROP 75°).

irradiance at the surface have a better STDVM than the corresponding values for the low AOT case (Table 3a, column 8). Referring back to the absorptance at low AOT (Table 3a), inspection of columns 7 and 9 in Tables 2 and 3a shows that the disagreement in broadband absorptance among models is higher for a molecular case for a SZA of 75°, indicating that the problem lies in the parameterization of gaseous absorption among the models, or possibly in difficulties in switching off absorption by minor gases (whose effects become pronounced for the longer path lengths) as required by the protocol.

2.3. Aerosol Forcing Calculations From Cases 1 and 2

[21] Aerosol forcing calculations from Cases 1 and 2, summarized in Tables 3c and 3d, show that models are in fairly close agreement (STDVM 5–14%) for broadband $E_S^{\downarrow}$ and $E_S^{\uparrow}$ SAW atmosphere and broadband $E_S^{\downarrow}$ for the TROP atmosphere but not for the broadband $E_S^{\uparrow}$ computation for the TROP atmosphere (STDVM 20–75%), with a few models being clear outliers (not shown). For the three broadband irradiance components, $E_{TOA}^{\uparrow}$, $E_S^{\downarrow}$ and $E_S^{\uparrow}$, they are also plotted as a function of SZA and AOT (Figures 2e, 2f, and 2g) and the component, $E_{TOA}^{\uparrow}$ is plotted as a function of AOT for a fixed SZA (30°, Figure 2h). For most models the magnitude of the forcing increases somewhat with increase in SZA from 30° to 75°. Such an increase in forcing is expected for an optically thin atmosphere because of increased upscatter fraction, the decrease in incident irradiance (which varies as cos θ_0) being compensated by the increase in path optical thickness that varies as sec θ_0 [*Nemesure et al.*, 1995]. Such a behavior was systematically exhibited by the several models that participated in the intercomparison study of *Boucher et al.* [1998]. For constant aerosol properties the forcing should, to first order, vary linearly with AOT, approaching zero as AOT goes to zero (Figure 2h). Because the present intercomparison specified somewhat different aerosol properties at the two values of AOT examined (0.08 and 0.24 at 550 nm), an exact linear dependence of forcing on AOT is not to be expected in the present study. Still, most of the models reflected a dependence of forcing on AOT that was fairly linear in AOT (including the zero AOT point), again with one exception (M14, Figure 2h). On the basis of this limited comparison, more systematic examination of the linearity of

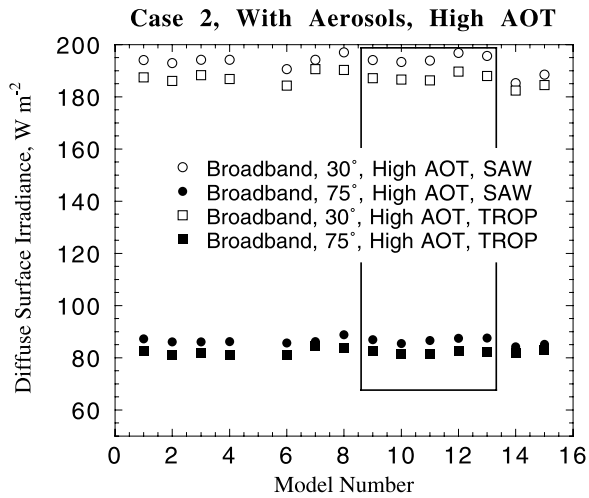

Figure 2c. The agreement here for the "high AOT" Case 2 in the computation of E_{dif} (broadband) is one of the best. The STDVM for the four cases shown here are 1.65, 1.36, 1.24, and 1.24 for the 30° SAW, 75° SAW, 30° TROP, and 75° TROP cases, respectively.

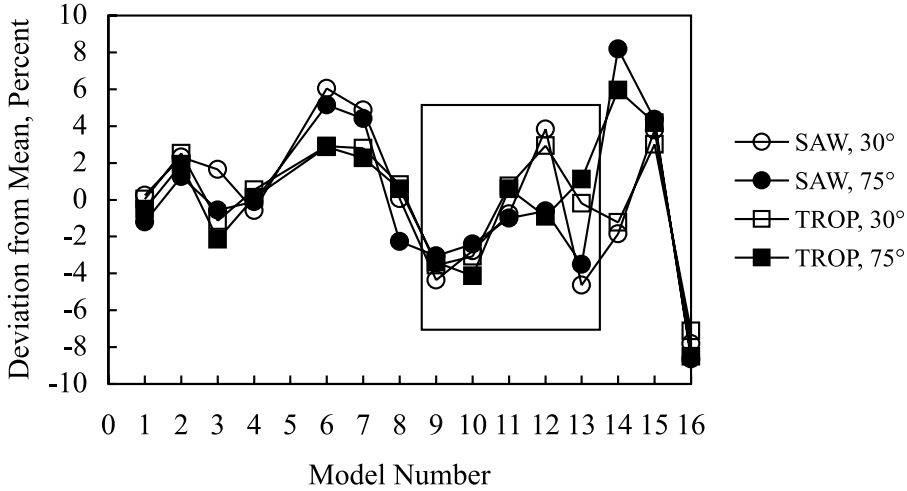

Figure 2d. Broadband absorptance as percent deviation from mean is plotted for the AOT (550 nm) = 0.24 case, SAW and TROP atmospheres, and two zenith angles. The STDVM is 3.4% for the 75° tropical atmospheric case (solid squares) with all the models included, and 2.8% with model 16 excluded (column 9, Table 3b). The mean values are: 0.14 (SAW 30°), 0.22 (SAW 75°), 0.22 (TROP 30°), and 0.31 (TROP 75°).

forcing with AOT would seem warranted in future intercomparisons.

2.4. Results for Case 3 (Comparison With Measurements)

[22] Results for Case 3 (comparison with measurements) confirmed what was usually observed at the time of formulation of this study: that the model computations generally exceeded measured values of diffuse irradiance, by a margin that could not be accounted for by measurement uncertainties, while correctly calculating direct irradiance (Table 4, Figure 3a, *Kato et al.* [1997], and *Halthore and Schwartz* [2000]). This was taken to mean that all the models participating in this study had insufficient shortwave absorption, to varying degrees, for a proper simultaneous closure of direct and diffuse irradiance. A possible explanation is that a continuum absorber, most likely in the form of aerosol absorption, is causing the excess absorption (relative to models) in cloud-free skies, as in this case. The observed excess absorption, if due to aerosols, is probably indicative of the presence of black carbon, soot, or other dark organic aerosol. All models depict this need for excess atmospheric absorption to properly "close" downward surface direct and diffuse irradiance simultaneously.

[23] The need for additional absorption is most apparent for the low AOT case (Figure 3a); for the high AOT case, small differences in modeled and actual aerosol scattering properties could have easily brought the model values closer to the measurement. Also, the agreement among models is generally seen to be best for the high AOT case (column 7 compared with column 6 in Table 4), and this is an indication that the model disagreement becomes a smaller fraction of computed quantities of irradiance for high AOT. Figure 3b shows considerable scatter in the computed broadband absorptance that is reflected in STDVM values (Table 4, column 6 compared with column 7).

2.5. Results for Case 4 (Cloud Case)

[24] Results for Case 4 (cloud case), summarized in Table 5, show that the number of models providing results

Table 3c. Cases 1 and 2, Aerosol Forcing, Average Values[a]

		Subarctic Winter				Tropical			
		Low AOT		High AOT		Low AOT		High AOT	
Irradiance Component	Wavelength	30° SZA	75° SZA	30° SZA	75° SZA	30° SZA	75° SZA	30° SZA	75° SZA
Upward flux at TOA	Broadband	1.18	9.41	3.93	18.23	1.54	9.15	4.41	17.73
Upward flux at TOA	0.20–0.35	0.03	0.02	0.16	0.09	0.02	0.03	0.16	0.09
Upward flux at TOA	0.35–0.70	0.70	4.13	2.77	9.79	0.69	4.25	2.85	10.08
Upward flux at TOA	0.70–5.00	0.44	5.33	0.90	8.51	0.78	4.90	1.27	7.64
Total down at surface	Broadband	−12.26	−18.38	−33.03	−38.57	−11.64	−15.86	−32.10	−34.76
Total down at surface	0.20–0.35	−0.44	−0.13	−1.98	−0.46	−0.46	−0.15	−2.10	−0.48
Total down at surface	0.35–0.70	−6.24	−8.83	−21.44	−22.59	−6.28	−8.82	−21.59	−22.54
Total down at surface	0.70–5.00	−5.59	−9.54	−9.73	−15.89	−4.65	−7.02	−8.58	−12.06
Diffuse up at surface	Broadband	−2.40	−3.65	−6.59	−7.75	−1.95	−2.87	−6.12	−6.71
Diffuse up at surface	0.20–0.35	−0.09	−0.02	−0.40	−0.11	−0.10	−0.03	−0.42	−0.12
Diffuse up at surface	0.35–0.70	−1.24	−1.78	−4.28	−4.53	−1.26	−1.77	−4.32	−4.52
Diffuse up at surface	0.70–5.00	−1.05	−1.85	−1.89	−3.11	−0.60	−1.06	−1.39	−2.08

[a]In this and subsequent tables, "Broadband" refers to the range 0.28–5.00 μm.

Table 3d. Cases 1 and 2, Aerosol Forcing, Percent STDVM

		Subarctic Winter				Tropical			
		Low AOT		High AOT		Low AOT		High AOT	
Irradiance Component	Wavelength	30° SZA	75° SZA	30° SZA	75° SZA	30° SZA	75° SZA	30° SZA	75° SZA
Upward flux at TOA	Broadband	59.80	7.80	27.30	4.90	62.00	12.70	27.90	8.20
Upward flux at TOA	0.20–0.35	107.90	112.60	45.50	52.00	198.80	113.00	59.00	65.50
Upward flux at TOA	0.35–0.70	51.40	9.10	22.30	2.20	45.30	8.80	20.80	2.00
Upward flux at TOA	0.70–5.00	96.60	9.40	53.80	10.60	104.30	21.00	70.20	19.80
Total down at surface	Broadband	5.00	5.90	5.10	5.20	14.40	9.20	6.10	6.30
Total down at surface	0.20–0.35	12.60	35.70	13.00	27.90	15.10	28.80	13.20	25.90
Total down at surface	0.35–0.70	5.90	8.90	7.30	5.30	5.90	8.70	7.20	5.30
Total down at surface	0.70–5.00	7.60	3.20	7.00	3.40	23.50	15.30	14.40	9.00
Diffuse up at surface	Broadband	11.70	8.90	6.40	4.30	74.80	51.70	24.60	22.10
Diffuse up at surface	0.20–0.35	31.40	86.80	12.60	27.00	7.20	89.70	13.30	26.40
Diffuse up at surface	0.35–0.70	6.10	8.90	7.40	5.50	4.50	9.20	7.10	5.40
Diffuse up at surface	0.70–5.00	24.70	13.60	15.20	8.30	243.00	137.00	105.20	70.10

for this case dropped to 11, perhaps because of the difficulty in specifying cloud properties in several of the models. Remarkably, the agreement among models for the computation of $E^{\uparrow}_{TOA}$ (segments e and f in Figure 4) is found to be excellent (0.77% and 1.09% STDVM for SZAs 30° and 75° respectively) while that for the broadband absorptance (segments g and h in Figure 4) is relatively poor (1.85% and 2.37% for 30° and 75°, respectively).

[25] Considering that the cloud attenuation was very high (direct component was zero at the surface), the agreement among models for the computation of diffuse components at the surface and at TOA is surprisingly good, especially for low SZA. The STDVM for the larger SZA is higher than that for the lower SZA, but this is to be expected. In Figure 4, M15 shows maximum deviation (segments b and d in Figure 4 corresponding to surface fluxes at 75° SZA) from the rest of the models, perhaps because of its use of updated water vapor absorption coefficients. An encouraging aspect here is the relatively good agreement among models for the atmospheric absorptance that shows low STDVM for the broadband (1.85% and 2.37%, for SZA of 30° and 75°, respectively). In the *Barker et al.* [2003] study, the two line-by-line models and the four 3-D Monte Carlo photon transport models (comprising their benchmark calculations) all agreed to within ±2% for the estimates of atmospheric absorptance, top-of-atmosphere albedo, and surface absorptance, consistent with present findings.

[26] Cloud alteration of absorption (Table 6) can be studied because Case 4 is essentially the same as the tropical atmosphere in Case1 but with the inclusion of a cloud. The enhancement in absorptance is noticeably large (30%) for the low zenith angle case, whereas it is relatively small (3%) for the high zenith angle case. A possible explanation is that at high solar zenith angle, the absorption lines get saturated in the part of the atmosphere above the clouds, leaving relatively small amount of energy for absorption in the clouds.

3. Conclusions

[27] The agreement among models is much better here than that for a similar study conducted about 13 years ago [*Fouquart et al.*, 1991]. However, rather than this being due to any inherent improvement in multiple scattering schemes, we attribute this to better specification and utilization of input parameters and treatment of atmospheric absorption. Using the results of a study done some years ago involving comparison in the computed fluxes and radiances by different methods of solution to the transfer equation including "exact" methods, *Lenoble* [1985] reports agreement to within 1%. Here the agreement among models for broadband total surface irradiance for a molecular atmosphere is generally better than 2% for the irradiances and better than the 1–3% STDVM result in the study of *Fouquart et al.* [1991]. The STDVM for absorptance is likewise much improved (2–5% compared with 6 to 11%).

[28] With addition of aerosols, the results are similar to those of the aerosol-free case, with reasonable agreement in some components, but curiously better agreement in some others (e.g., $E^{\uparrow}_{S}$ at the surface for the low AOT case). As expected, the higher AOT case depicts slightly poorer agreement than the aerosol-free case for all components. An exception is broadband $E^{\uparrow}_{TOA}$ for which there is better agreement among models for both the SAW and tropical atmospheres for a solar zenith angle of 30°. Almost all models depict positive aerosol forcing for $E^{\uparrow}_{TOA}$ (i.e., cooling effect), negative forcing for $E^{\downarrow}_{S}$, and

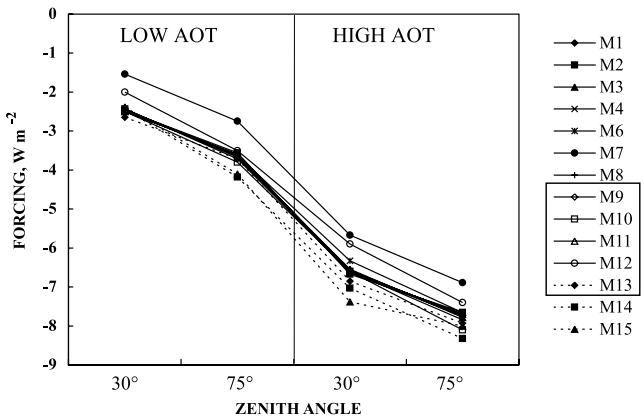

Figure 2e. For a SAW atmosphere, broadband aerosol forcing at the surface for upward flux at surface $E^{\uparrow}_{S}$ is shown here as a function of AOT and zenith angle.

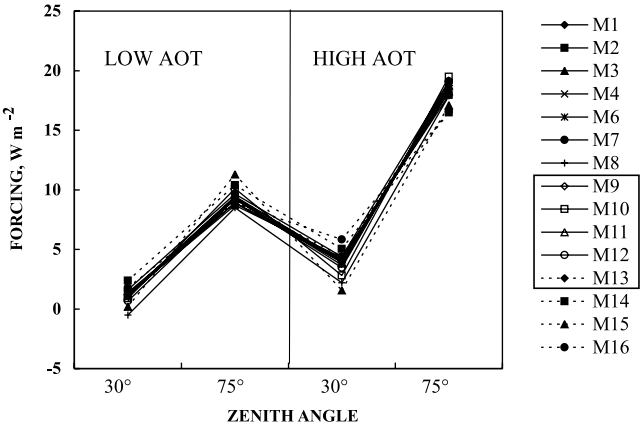

Figure 2f. For SAW atmosphere, figure shows aerosol forcing of broadband $E^{\uparrow}_{TOA}$ as a function of SZA and low and high values of AOT. The values for TROP atmosphere are substantially similar.

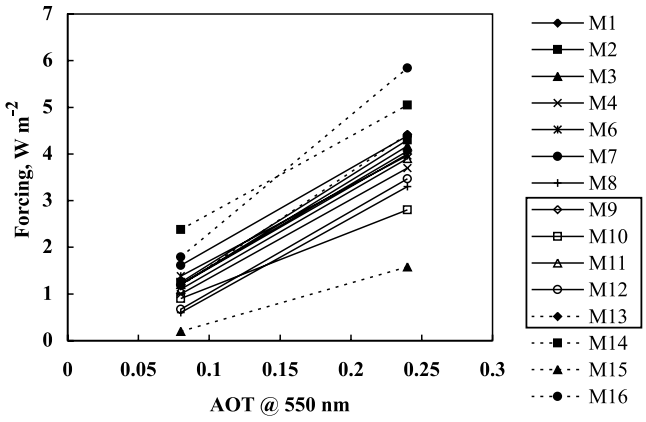

Figure 2h. Dependence of aerosol forcing of the quantity $E^{\uparrow}_{TOA}$ on aerosol optical thickness at fixed SZA of 30° and a SAW atmosphere.

negative forcing for $E^{\uparrow}_{S}$ (i.e., aerosols decrease surface irradiance because aerosols increase upward scatter). The magnitude of the forcing generally scales with AOT for all components.

[29] In the case of model comparison with measurements, all models agree to better than 3% in the broadband calculations of irradiance, but the absorptance has a larger spread for the low AOT case (8.45%) than for the high AOT case (3.17%). Model calculations for specific regions of the spectrum, UV, VIS and IR, generally have a much larger spread than for the broadband. All models overpredict $E^{\downarrow}_{dif}$ at the surface for the low AOT case and assume aerosol scattering properties when compared with measured values while correctly calculating $E^{\downarrow}_{dir}$. If, as recent evidence suggests, low values of aerosol single scattering albedos are used, results of all models could be made to achieve closure with measured values. For the high AOT case, closure is achieved, but here all models are more sensitive to assumed and measured aerosol scattering properties. Computation of $E^{\uparrow}_{TOA}$, which is of relevance to satellite sensor calibration, has STDVMs of 1–3%.

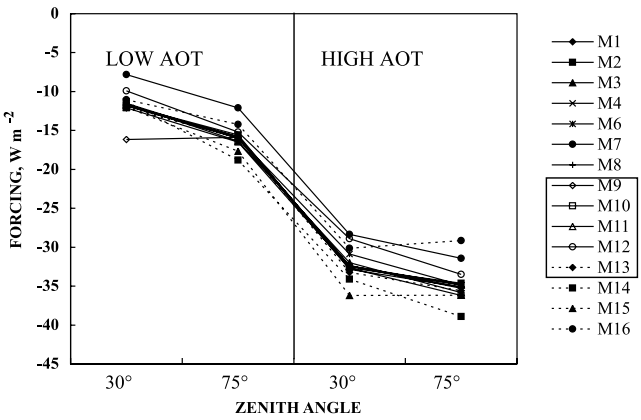

Figure 2g. For TROP atmosphere, figure shows aerosol forcing of the broadband surface irradiance $E^{\downarrow}_{S}$ as a function of AOT and zenith angle. (Forcing here is a strong function of AOT unlike in the previous case.)

[30] In the presence of cloud, absorption is enhanced relative cloud-free skies by 30% at 30° SZA, but there is virtually no enhancement at 75°. Broadband absorptance (cloud plus atmosphere) is calculated to within 2.5% by the models. The sources of uncertainty in the computations are most likely in the vertical resolution, varying wavelength resolution, varying extent of the line-width cutoff for the line-by-line models, and finally, the parameterization of gaseous continuum absorption. The sole GCM taking part in this study provided values comparable to those of the other codes. With the solution for the atmospheric excess absorption problem almost realized in clouds [*Ackerman et al.*, 2003] [see also *Valero et al.*, 2004; *Halthore et al.*, 1998], it is expected that the detailed radiative schemes, when incorporated into GCMs, will provide better simulations of the climate and of weather phenomena.

Appendix A: Description of Models

[31] A brief description of each of the models used in this intercomparison is given below; a summary of the model characteristics is given in Table 1. For details on radiative transfer theory and descriptions of various methods for solving the transfer equation, we refer the reader to the references given for each model as well as some general references [*Chandrasekhar*, 1960; *van de Hulst*, 1980; *Lenoble*, 1985; *Liou*, 1992]. The names of investigators who reported results from these models are given in parentheses in the title line for each model. In some cases the investigators actually developed the models; in others, they are some of the principal users of those models that someone else developed.

A1. Model 1: Atmospheric Radiation Code (ATRAD2) (Investigators I. Laszlo and W. Wiscombe)

[32] Developed by W. Wiscombe and colleagues in the 1970s, the model calculates flux in a vertically inhomogeneous scattering-absorbing atmosphere using the adding-doubling (D-A) method [*Hunt and Grant*, 1969], and accounts for the absorption of all radiatively important gases using exponential fits to the LOWTRAN-7 transmittances [*Wiscombe et al.*, 1984; *Laszlo*, 1994]. In addition

Table 4. Case 3, Comparison With Measurements

	Measurements		Average		Standard Deviation As a % of Mean	
	0.08[a]	0.24[a]	0.08[a]	0.24[a]	0.08[a]	0.24[a]
	27.08° SZA	51.39° SZA	27.08° SZA	51.39° SZA	27.08° SZA	51.39° SZA
			Direct Down			
0.28–5.00, μm	862	436	869.53	444.03	1.25	0.90
0.20–0.35, μm			11.14	2.53	4.36	5.24
0.35–0.70, μm			393.38	184.75	1.21	0.74
0.70–5.00, μm			464.89	256.72	1.40	1.44
			Diffuse Down			
0.28–5.00, μm	88	141	113.50	143.85	1.85	0.82
0.20–0.35, μm			9.18	7.31	4.38	6.90
0.35–0.70, μm			75.74	101.37	1.79	0.70
0.70–5.00, μm			28.58	35.16	2.37	1.79
			Diffuse Up			
0.28–5.00, μm			211.94	126.55	1.77	1.85
0.20–0.35, μm			1.04	0.51	12.21	12.44
0.35–0.70, μm			54.60	33.49	1.86	1.57
0.70–5.00, μm			156.28	92.55	1.90	2.14
			Diffuse Up TOA			
0.28–5.00, μm			238.45	169.81	2.43	1.76
0.20–0.35, μm			8.33	7.09	7.40	8.05
0.35–0.70, μm			88.26	76.28	2.63	2.71
0.70–5.00, μm			141.86	86.46	2.88	3.01
			Absorptance			
0.28–5.00, μm			15.68	25.44	8.45	3.17
0.20–0.35, μm			45.22	53.93	5.01	5.05
0.35–0.70, μm			2.68	9.97	45.28	8.46
0.70–5.00, μm			24.89	36.64	4.64	2.37

[a]AOT at 550 nm.

to the present study, the model has been tested against limited observations. It has also contributed to participation in a number of intercomparison efforts [*Wiscombe et al.*, 1984; *Laszlo et al.*, 1988; *Fouquart et al.*, 1991; *Boucher et al.*, 1998].

[33] Absorption by H_2O, CO_2, and O_3 were included in all cases. In addition to these gases, Case 3 had O_2, N_2O, CO, and CH_4, while Case 4 included O_2. This model used 199 spectral intervals between 200 and 5000 nm. In this model, vertical resolution can be adjusted as needed (39 levels for Cases 1 and 2, 36 levels for Case 3, and 41 levels for Case 4). In all cases with aerosol, the optical properties of aerosol were calculated explicitly at the model wavelengths. The aerosol cases were calculated using a Henyey-Greenstein phase function obtained from the asymmetry parameter that was provided. In Case 4 the full phase function was reconstructed from the Legendre moments provided. The spectral fluxes calculated at the model spectral intervals were interpolated to the intervals used in the intercomparison.

A2. Model 2: A-D Model With MODTRAN-3.5 Transmittance (A. Trishchenko and Z. Li)

[34] On the basis of doubling-adding radiative transfer code developed by *Masuda et al.* [1995], the model uses Modtran 3.5 atmospheric trasmittance in 105 unequal spectral intervals within the range 0.25–5 μm. The lower limit of 0.28 μm was used in this study according to protocol. Doubling-adding radiative transfer scheme uses 22 streams (11 up and 11 down) and 8 layers in the atmosphere: 0–1 km, 1–2 km, 2–4 km, 4–6 km, 6–9 km, 9–13 km, 13–25 km, and 25–100 km. A nitrogen-oxygen atmosphere included water, ozone, and carbon dioxide for minor gases as specified by Modtran 3.5 sub-arctic winter (SAW) and tropical (TROP) built-in models. All other gases were neglected, except for Case 3 for comparison with real observations. Calculations for Case 4 (cloudy atmosphere) were also compared to the computations with cloud optical properties generated using refractive index values of water from *Hale and Querry* [1973]. A check

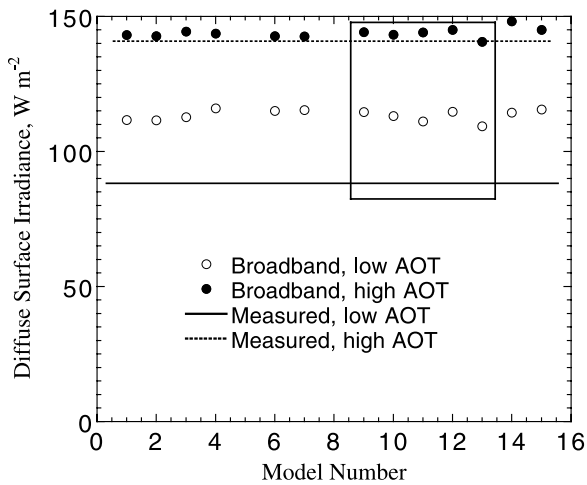

Figure 3a. Comparison of model calculated diffuse surface irradiance (broadband) and measured values for two cases: high and low AOT.

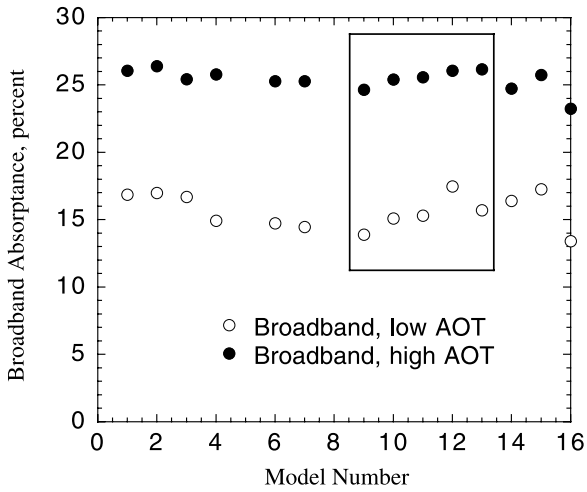

Figure 3b. Comparison of absorptance in models for the two cases (high and low AOT) shown in Figure 3a.

yielded a difference in SW fluxes of less than ~5 W m^{-2}. The model used H-G phase function with specified asymmetry parameter.

A3. Model 3: A-D Model With LOWTRAN 7 Transmittance (F. Chang)

[35] On the basis of a doubling-adding code [see *Chang et al.*, 2000; *Chang*, 1997] the model uses a 32-stream (16 up and 16 down) computation for radiative transfer. The atmosphere is divided into seven vertical layers, 0–1 km, 1–2 km, 2–4 km, 4–7 km, 7–12 km, 12–25 km, and 25–100 km, and transmittances are based on the LOWTRAN7 model. The spectrum is divided into a total of 112 bands with variable bandwidths in the range 0.25–5.0 μm. In particular, the wavelength resolution is about 0.005–0.01 μm for wavelength less than 0.365 μm, 0.01–0.1 μm for wavelengths in the range 0.365–2.2 μm, and 0.1 μm in the range 2.2–5.0 μm. The model has been used to examine the relationship between cloud and radiation quantities derived from satellite observations and model calculations [*Chang et al.*, 2000].

A4. Models 4 and 5: GAME, a Correlated k-Distribution Model With DISORT (P. Dubuisson, B. Bonnel, O. Boucher, and Y. Fouquart)

[36] GAME is a radiative transfer code for radiance or irradiance calculations in plane-parallel atmospheres, with various spectral resolutions (Model 4: 10 cm^{-1}; Model 5: 100 or 400 cm^{-1}). Gaseous absorption by water vapor, oxygen, and carbon dioxide is calculated by a correlated k-distribution method [*Lacis and Oinas*, 1991]. Coefficients of exponential series are conveniently calculated using the Malkmus band model [*Malkmus*, 1967]. Band parameters are directly estimated by least squares fitting the Malkmus band model with line-by-line calculations (see Model 11) at reference pressure and temperature conditions. The scaling approximation [*Stephens*, 1984] is applied to account for the vertical dependence of the absorption. Ozone and water vapor absorption continuum are also included using the CKD2.4 parameterization [*Clough et al.*, 1989]. The models use the Discrete Ordinate Radiative Transfer (DISORT) method [*Stamnes et al.*, 1988] to solve the radiative transfer equation. The GAME code also accounts for molecular, cloud, and

Table 5. Case 4, Cloud With Tropical Atmosphere

	Average		Standard Deviation as % of Mean	
	30° SZA	75° SZA	30° SZA	75° SZA
		Direct Down		
Broadband	0	0	0	0
0.20–0.35	0	0	0	0
0.35–0.70	0	0	0	0
0.70–5.00	0	0	0	0
		Diffuse Down		
Broadband	150.5	24.4	1.52	5.44
0.20–0.35	5	0.7	1.23	2.63
0.35–0.70	92.8	15	0.75	1.09
0.70–5.00	52.7	8.7	4.57	16.03
		Diffuse Up		
Broadband	30.1	4.9	1.52	5.67
0.20–0.35	1	0.1	1.07	15.81
0.35–0.70	18.6	3	0.76	1.04
0.70–5.00	10.5	1.7	4.59	15.94
		Diffuse Up TOA		
Broadband	746.7	231	0.77	1.09
0.20–0.35	21.2	6.1	2.15	3
0.35–0.70	407.5	125.5	0.38	0.57
0.70–5.00	317.9	99.5	1.65	2.39
		Absorptance		
Broadband	26.40	28.82	1.85	2.37
0.20–0.35	49.02	55.00	1.96	2.32
0.35–0.70	5.02	9.27	9.32	6.26
0.70–5.00	42.55	43.18	1.87	3.32

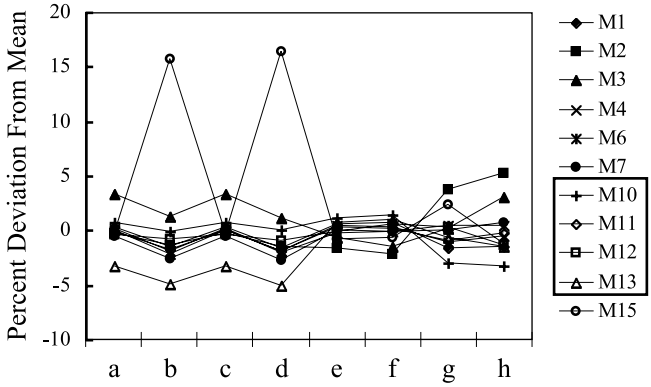

Figure 4. For the cloud case, model computation of broadband fluxes and broadband absorptance are compared for (segment a) $E_S^{\downarrow}$, 30° SZA, (segment b) $E_S^{\downarrow}$, 75° SZA, (segment c) $E_S^{\uparrow}$, 30°, (segment d) $E_S^{\uparrow}$, 75° SZA, (segment e) $E_{TOA}^{\uparrow}$, 30° SZA, (segment f) $E_{TOA}^{\uparrow}$, 75° SZA (segment g) A, 30° SZA and (segment h) A, 75° SZA, as percent deviation from mean. The mean values are: (segment a) 150.48 W m^{-2}, (segment b) 24.44 W m^{-2}, (segment c) 30.1 W m^{-2}, (segment d) 4.9 W m^{-2}, (segment e) 746.7 W m^{-2}, (segment f) 231.0 W m^{-2}, (segment g) 0.264, and (segment h) 0.288.

aerosol scattering. It should be noted that results for Model 5 are only shown for Case 1 since for other cases, results of the higher resolution Model 4 are more accurate.

A5. Model 6: Santa Barbara DISORT Atmospheric Radiative Transfer Model (SBDART) (P. Richiazzi, S. Yang, and C. Gautier)

[37] SBDART [*Ricchiazzi et al.*, 1998] is a general purpose, plane-parallel radiative transfer model for use in both clear and cloudy conditions within the Earth's atmosphere. The code is well suited to handle a wide variety of problems in atmospheric radiative energy balance and remote sensing in the shortwave and longwave spectral range. The SBDART source code is available by anonymous FTP (ftp://ftp.icess.ucsb.edu/pub/esrg/sbdart/sbdart_2.3.tar.gz), and a demo version runs on the World Wide Web (http://arm.mrcsb.com/sbdart/).

[38] SBDART relies on low-resolution band models developed for the LOWTRAN-7 atmospheric transmission code [*Pierluissi and Maragoudakis*, 1986]. These band models provide clear sky atmospheric transmission from 0 to 50,000 cm^{-1} at 20 cm^{-1} resolution and include the effects of all radiatively important molecular species found in the Earth's atmosphere. The transmission functions are approximated with a three-term exponential fit [*Wiscombe and Evans*, 1977]. The radiative transfer equation is numerically integrated with the DISORT [*Stamnes et al.*, 1988] radiative transfer module. The intensity of both scattered and thermally emitted radiation can be computed at different heights and directions.

[39] The standard configuration allows up to 65 atmospheric layers and 40 radiation streams (40 zenith angles and 40 azimuth modes). For the results presented here, SBDART was run with 33 altitude layers (1 km resolution in the troposphere) and used eight radiation streams. For Case 2 (aerosols) the specified phase function was expanded in terms of Legendre moments, and truncated to eight terms using the delta-M method [*Wiscombe*, 1977]. A Henyey-Greenstein phase function was used for Case 4 (cloud). For this case, scattering properties (extinction efficiency, single scattering albedo, and asymmetry factor) were obtained by interpolation on SBDART's internal database assuming a cloud drop effective radius of 5 μm.

A6. Model 7: Santa Barbara Moderate Resolution (SBMOD) Radiative Transfer Algorithm (P. Richiazzi, S. Yang, and C. Gautier)

[40] SBMOD [*Yang et al.*, 1999] performs radiative transfer at a wavelength resolution of 1 nm. It uses a k-distribution lookup table based on the HITRAN line database. The lookup table covers the spectral range between 0.25 and 5 μm and contains entries for a range of temperatures, pressures, and mixing ratio of water vapor and ozone. Up to 16 k-distribution terms are used to model the transmission within each wavelength step. SBMOD uses the same cloud, aerosol, and surface models as SBDART.

A7. Model 8: A Delta-Four-Stream Approximation Model (RAPRAD) (S. Kato, E. E. Clothiaux, and J. H. Mather)

[41] Results of the model based on delta-four-stream approximation for radiative transfer [*Liou et al.*, 1988] are presented. The model uses a k-distribution method [*Kato et al.*, 1999] to characterize molecular absorptions arising from water vapor (including continuum), ozone, oxygen, and carbon dioxide. A total of 32 wavelength intervals span the solar spectrum (0.24–4.6 μm). The molecular database is based on HITRAN92. Initial comparison of the results of this model with MODTRAN3 demonstrates that the spectral transmittance is within 0.01 throughout most of the solar spectrum. Atmosphere is divided into 17 vertical layers with pressure decreasing in geometric progression with altitude.

[42] RAPRAD is developed to compute the vertical irradiance profile in the atmosphere for both shortwave and longwave regions. It also provides computation based on a two-stream algorithm given by *Toon et al.* [1989]. The longwave region from 3.3 μm to 1000 μm is divided into 16 bands. For the longwave, k-distribution table given by

Table 6. Absorptance in Cloudy and Cloud-Free Atmospheres

	Absorptance, Cloudy Atmosphere (Case 4)		Absorptance, Cloud-Free Atmosphere (Case 1)	
	30° SZA	75° SZA	30° SZA	75° SZA
Broadband	0.264	0.288	0.205	0.281
0.20–0.35	0.490	0.550	0.449	0.536
0.35–0.70	0.050	0.093	0.033	0.082
0.70–5.00	0.425	0.432	0.332	0.428

Mlawer et al. [1997] is used along with correlated-k assumption to compute absorption.

A8. Model 9: A Line-by-Line Model With Discrete-Ordinate Method (M. D. Chou)

[43] The line-by-line model employs the discrete-ordinate (DISORT) method to solve the transfer equation and compute fluxes. It includes Rayleigh scattering and absorption by water vapor, ozone, carbon dioxide, and oxygen. The spectral range extends from 0.2 to 10.0 μm instead of from 0.2 to 5.0 μm as was specified. It was noted that in the band from 0.2 to 0.28 μm, the ozone absorption is very strong and the insolation at the TOA is very small (∼1 W m^{-2} for the SZA of 30° and 75°). This band has a negligible effect on the fluxes both at the surface and at the TOA. Calculations are performed using the detailed aerosol scattering phase function that was specified in the protocol.

A9. Model 10: A Line-by-Line Model With Doubling-Adding Method (S. Freidenreich and V. Ramaswamy)

[44] The method is based on a doubling-adding solution to the transfer equation [*Hunt and Grant*, 1969; *Ramaswamy and Freidenreich*, 1991; *Freidenreich and Ramaswamy*, 1999]. The model is discussed in detail in the latter two references; a few salient points are given here. In this exercise, the model employs 32 streams for computing the fluxes. The line-by-line method is used for the portion of the solar spectrum for which line parameter data are available (0–22,700 cm^{-1} and 44,100–57,600 cm^{-1}) while a 1 cm^{-1} spectral resolution is used otherwise. Molecular absorption parameters (for CO_2, water vapor, and O_2) for both the spectral regions are from the HITRAN database [*Rothman et al.*, 1992; L. S. Rothman, private communication, 1997]; water vapor continuum is not included. The atmosphere is divided into 122 layers and spanning pressure levels from 10^{-3} to 1013.25 mbar. O_3 parameters are from the WMO report [*World Meteorological Organization*, 1986], with an update in the UV range provided using the JPL report [*Jet Propulsion Laboratory*, 1992].

A10. Model 11: GAME, a Line-By-Line Model With Discrete Ordinate Method (P. Dubuisson, B. Bonnel, O. Boucher, and Y. Fouquart)

[45] This high spectral resolution radiative transfer code, referred to as the GAME code [*Dubuisson et al.*, 1996], is based on the coupling of a line-by-line code and an accurate method to solve the radiative transfer equation in the assumption of a vertically inhomogeneous atmosphere stratified into plane and parallel layers. Monochromatic absorption coefficients are calculated with a line-by-line (LBL) code originally developed in the longwave spectral region [*Scott*, 1974] and adapted to the solar spectrum. Water vapor absorption lines are calculated using the Hitran-2000 spectroscopic database [*Rothman et al.*, 2003]. The CKD2.4 parameterization is used for the water vapor absorption continuum [*Clough et al.*, 1989]. Ozone absorption continuum in the visible and UV spectral region is also included. The radiative transfer equation is solved at each wavelength step of the LBL code from the Discrete Ordinate Method (DOM) [*Stamnes et al.*, 1988]. The GAME code accounts for Rayleigh scattering, as well as cloud or aerosol scattering using the following optical properties for each atmospheric layer: the moments of the phase function, the single scattering albedo, and the extinction optical thickness. For both GAME models 4 and 11, cloud properties (single scattering albedo, extinction coefficient and moments of the phase function) were defined at 208 wavelengths between 0.2 and 5 μm.

A11. Model 12: A Line-by-Line Model With Discrete Ordinate Method (D. Crisp)

[46] The model uses H_2O continuum from *Clough et al.* [1989] and a Voigt line shape profile for line-center distances less than 40 times the Doppler half-width; at larger distances, a Van Vleck–Weisskopf profile [*Meadows and Crisp*, 1996] was used. The line cutoff distance for H_2O was typically 1000 cm^{-1}; for all other gases it was 500 cm^{-1}. Spectral line parameters from the HITRAN-96 database were used for all gases at near-infrared wavelengths. UV and visible absorption cross sections were derived from *DeMore et al.* [1992]. The model uses a multilevel, multistream, discrete-ordinate algorithm, DISORT [*Stamnes et al.*, 1988] to generate altitude- and angle-dependent solar radiances at each wavelength. It calculates monochromatic radiances for 4 to 32 zenith angles (or streams) at 62 levels between the surface and 80 km to compute fluxes. This model was used in the study of the excess absorption anomaly [*Crisp*, 1997].

A12. Model 13: A Line-by-Line Model With Monte Carlo Method (B. Fomin and A. Plana-Fattori)

[47] This line-by-line model uses the HITRAN-96 spectral database and the *Clough et al.* [1989] continuum models for water vapor, oxygen, and ozone from LOWTRAN-7 [*Fomin*, 1995]. It calculates optical properties of clouds and aerosols using Mie theory and an approach based on geometric optics (in the case of large particles). Flux is calculated in a vertically inhomogeneous scattering-absorbing atmosphere using a rigorous Monte Carlo method [*Fomin and Mazin*, 1998]. This model has been used for creating a database of benchmark calculations for the Intercomparison of Radiation Codes in Climate Models (ICRCCM) program test cases [*Fomin and Gershanow*, 1997] which was also recommended for broadband code validation by the Radiative Panel of Global Energy and Water Cycle Experiment (GEWEX), Honolulu, Hawaii, July 22–25, 1997.

[48] Here vertical resolution used was the same as that in the initial atmospheric models, 50 vertical levels. The aerosol cases were calculated using a Henyey-Greenstein function for the specified parameters. For Case 4, a phase function (at 421 angles) and scattering/absorption coefficients of cloud were calculated at ∼150 wavelengths, which were defined by the specified table of water refractive indices. All other information was used in these calculations without any further simplifying assumptions.

A13. Model 14: MODTRAN-4, a Broadband Model With Two Stream Approximation (R. Halthore, G. P. Anderson, A. Berk, and S. E. Schwartz)

[49] The widely used MODTRAN (short for MODerate resolution radiative TRANsfer program) code [*Berk et al.*,

1998] is the latest version of a long list of radiative transfer models developed by scientists associated with the Air Force Geophysical Laboratory at Hanscom Air Force Base, in Massachusetts. The model calculates multiply scattered radiance accounting for the curvature of the Earth, refractive geometry effects, and a general scattering phase function. MODTRAN allows multiple-scattering calculations using a two-stream approximation based on Isaacs' method [*Isaacs et al.*, 1987] and an adding method for combining atmospheric layers [*Berk et al.*, 1998]. An initial estimate of the errors due to the multiple scattering parameterization for solar and thermal radiance calculations was less than 10%. This model is generally used when speed of computation is a factor. For more accuracy, Model 15 (described next), available in the same code, is used.

A14. Model 15: MODTRAN-4, a Broad Band Model With Discrete-Ordinate Method (Eight Stream) (R. Halthore, G. P. Anderson, A. Berk, and S. E. Schwartz)

[50] MODTRAN also allows computation of radiances and fluxes with the more accurate discrete ordinate (DISORT) method for multiple scattering calculations [*Stamnes et al.*, 1988]. The program was run with an effective spectral resolution of 2 cm^{-1} with eight streams of DISORT method. As with the previous case, the program uses band models based on HITRAN96 database with corrected water vapor absorption coefficients [*Giver et al.*, 2000]. For the vertical resolution, 50 altitude levels between the sea level and 120 km were used. Cloudy atmospheres can be modeled without including aerosols as was required in this study. For Case 4, cloud properties (extinction coefficient, absorption coefficient and the Henyey - Greenstein (H-G) asymmetry parameter) were specified at 188 wavelengths between 0.2 and 8.11 μm.

A15. Model 16: A General Circulation Model (M. D. Chou)

[51] Using a solar constant of 1373 Wm^{-2}, the GCM radiation model covering the spectral range from 0.2 to 10.0 μm computes the total irradiance at the surface and upward flux at the TOA. The surface albedo in each band is computed by taking the mean of the spectral surface albedo weighted by the insolation.

[52] **Acknowledgments.** We gratefully acknowledge Douglas L. Wright, Brookhaven National Laboratory, for providing aerosol optical properties for "urban average" aerosols with lognormal size distribution. We would also like to acknowledge Albert Arking, Johns Hopkins University, and an anonymous referee for their insightful comments on this paper.

References

Ackerman, T. P., D. M. Flynn, and R. T. Marchand (2003), Quantifying the magnitude of anomalous solar absorption, *J. Geophys. Res.*, *108*(D9), 4273, doi:10.1029/2002JD002674.

Anderson, G. P., S. A. Clough, F. X. Kneizys, J. H. Chetwynd, and E. P. Shettle (1986), AFGL Atmospheric Constituent Profiles (0–120 km), *Rep. AFGL-TR-86-0110*, Air Force Geophys. Lab., Hanscom AFB, Mass.

Barker, H. W., et al. (2003), Assessing 1D atmospheric solar radiative transfer models: Interpretation and handling of unresolved clouds, *J. Clim.*, *16*, 2676–2699.

Berk, A., L. S. Bernstein, G. P. Anderson, P. K. Acharya, D. C. Robertson, J. H. Chetwynd, and S. M. Adler-Golden (1998), MODTRAN cloud and multiple scattering upgrades with application to AVIRIS, *Remote Sens. Environ.*, *65*, 367–375.

Boucher, O., et al. (1998), Intercomparison of models representing direct shortwave radiative forcing by sulfate aerosols, *J. Geophys. Res.*, *103*, 16,979–16,998.

Chandrasekhar, S. (1960), *Radiative Transfer*, Dover, Mineola, N. Y.

Chang, F.-L. (1997), Properties of low-level marine clouds as deduced from AVHRR satellite observations, Ph.D. dissertation, 335 pp., Oregon State Univ., Corvallis, Oreg.

Chang, F.-L., Z. Li, and S. A. Ackerman (2000), Examining the relationship between cloud and radiation quantities derived from satellite observations and model calculations, *J. Clim.*, *13*, 3842–3859.

Clough, S. A., F. X. Kneizys, and R. W. Davies (1989), Line shape and the water vapor continuum, *Atmos. Res.*, *23*, 229–241.

Crisp, D. (1997), Absorption of sunlight by water vapor in cloudy conditions: A partial explanation for the cloud absorption anomaly, *Geophys. Res. Lett.*, *24*, 571–574.

DeMore, W., S. Sander, D. Golden, R. Hampson, M. Kurylo, C. Howard, A. Ravishankara, C. Kolb, and M. Molina (1992), Chemical kinetics and photochemical data for use in stratospheric modeling, *JPL Publ., 92-20*, 185 pp.

Dong, X., T. P. Ackerman, E. E. Clothiaux, P. Pilewskie, and Y. Han (1997), Microphysical and radiative properties of boundary layer stratiform clouds deduced from ground-based measurements, *J. Geophys. Res.*, *102*, 23,829–23,824.

Dubuisson, P., J. C. Buriez, and Y. Fouquart (1996), High spectral resolution solar radiative transfer in absorbing and scattering media: Application to the satellite simulation, *J. Quant. Spectrosc. Radiat. Transfer*, *55*, 103–126.

Fomin, B. A. (1995), Effective interpolation technique for line-by-line calculations of radiation absorption in gases, *J. Quant. Spectrosc. Radiat. Transfer*, *53*, 663–669.

Fomin, B. A., and Y. V. Gershanow (1997), Data bank on benchmark calculations of solar and longwave radiation fluxes in atmosphere for climate studies, in *Proceedings of IRS96: Current Problems in Atmospheric Radiation*, pp. 815–817, A. Deepak, Hampton, Va.

Fomin, B. A., and I. P. Mazin (1998), Model for an investigation of radiative transfer in cloudy atmosphere, *Atmos. Res.*, *47–48*, 127–153.

Fouquart, Y., B. Bonnel, and V. Ramaswamy (1991), Intercomparing shortwave radiation codes for climate studies, *J. Geophys. Res.*, *96*, 8955–8968.

Freidenreich, S. M., and V. Ramaswamy (1999), A new multiple-band solar radiative parameterization for general circulation models, *J. Geophys. Res.*, *104*, 31,389–31,409.

Giver, L. P., C. Chackerian, and P. Varanasi (2000), Visible and near-infrared $H_2{}^{16}O$ line intensity corrections for HITREAN-96, *J. Quant. Spectrosc. Radiat. Transfer*, *66*, 101–105.

Hale, G. M., and M. R. Querry (1973), Optical constants of water in the 200 nm to 200 μm wavelength region, *Appl. Opt.*, *12*, 555–563.

Halthore, R. N., and S. E. Schwartz (2000), Comparison of model estimated and measured diffuse downward surface irradiance in cloud-free skies, *J. Geophys. Res.*, *105*, 20,165–20,177.

Halthore, R. N., S. Nemesure, S. E. Schwartz, D. G. Imre, A. Berk, E. G. Dutton, and M. H. Bergin (1998), Models overestimate diffuse clear-sky surface irradiance: A case for excess atmospheric absorption, *Geophys. Res. Lett.*, *25*, 3591–3594.

Hunt, G. E., and I. P. Grant (1969), Discrete space theory of radiative transfer and its application to problems in planetary atmospheres, *J. Atmos. Sci.*, *26*, 963–972.

Intergovernmental Panel on Climate Change (2001), *Climate Change 2001: Working Group I: The Scientific Basis, IPCC Third Assessment Report*, edited by V. Ramaswamy et al., Cambridge Univ. Press, New York.

Isaacs, R. G., W. C. Wang, R. D. Worsham, and S. Goldenberg (1987), Multiple scattering LOWTRAN and FASCODE models, *Appl. Opt.*, *26*, 1272–1281.

Jet Propulsion Laboratory (1992), Chemical kinetics and photochemical data for use in stratospheric modeling: Evaluation, *JPL Publ., 92-20*, 185 pp.

Kato, S., et al. (1997), Uncertainties in modeled and measured clear-sky surface shortwave irradiances, *J Geophys. Res.*, *102*, 25,881–25,898.

Kato, S., T. P. Ackerman, J. H. Mather, and E. E. Clothiaux (1999), The k-distribution method and correlated-k approximation for a shortwave radiative transfer model, *J. Quant. Spectrosc. Radiat. Transfer*, *62*, 109–121.

Kurucz, R. L. (1994), Synthetic infrared spectra, in *Infrared Solar Physics: Proceedings of the 154th Symposium of the International Astronomical Union*, edited by D. M. Rabin, J. T. Jefferies, and C. Lindsey, pp. 523–531, Springer, New York.

Lacis, A. A., and V. Oinas (1991), A description of the correlated k-distribution method, *J. Geophys. Res.*, *96*, 9027–9064.

Laszlo, I. (1994), Calculation of longwave radiance spectra at a high resolution: Clear-sky results, in *Passive Infrared Remote Sensing of Clouds*

and the Atmosphere II, edited by D. K. Lynch, *Proc. SPIE Int. Soc. Opt. Eng.*, *2309*, 197–204.

Laszlo, I., H. Jacobowitz, and A. Gruber (1988), The relative merits of narrowband channels for estimating broadband albedos, *J. Atmos. Oceanic Technol.*, *5*, 757–773.

Lenoble, J. (1985), *Radiative Transfer in Scattering and Absorbing Atmospheres: Standard Computational Procedures*, A. Deepak, Hampton, Va.

Li, Z., L. Moreau, and A. Arking (1997), On solar energy disposition, A perspective from observation and modeling, *Bull. Am. Meteorol. Soc.*, *78*, 53–70.

Liou, K.-N. (1992), *Radiation and Cloud Processes in the Atmosphere*, Oxford Univ. Press, New York.

Liou, K.-N., Q. Fu, and T. P. Ackerman (1988), A simple formulation of the delta-four-stream approximation for radiative transfer parameterizations, *J Atmos. Sci.*, *45*, 1940–1947.

Malkmus, W. (1967), Random Lorentz band model with exponential-tailed S^{-1} line intensity distribution function, *J. Opt. Soc. Am. A Opt. Image Sci.*, *57*, 323–329.

Masuda, K., H. G. Leighton, and Z. Li (1995), A new parameterization for the determination of solar flux absorbed at the surface from satellite measurements, *J. Clim.*, *8*, 1615–1629.

Meadows, V. S., and D. Crisp (1996), Ground-based near-infrared observations of the Venus night side, *J. Geophys. Res.*, *101*, 4595–4622.

Mlawer, E. J., S. J. Taubman, P. D. Brown, M. J. Iacono, and S. A. Clough (1997), Radiative transfer for inhomogeneous atmospheres: RRTM, a validated correlated-*k* model for the longwave, *J. Geophys. Res.*, *102*, 16,663–16,682.

Nemesure, S., R. Wagener, and S. E. Schwartz (1995), Direct shortwave forcing of climate by the anthropogenic sulfate aerosol: Sensitivity to particle size, composition, and relative humidity, *J. Geophys. Res.*, *100*, 26,105–26,116.

Peixoto, J. P., and A. H. Oort (1992), *Physics of Climate*, Am. Inst. of Phys., College Park, Md.

Pierluissi, J. H., and C. E. Maragoudakis (1986), Molecular transmission band models for LOWTRAN, *AFGL-TR086-0272*, Hanscom AFB, Mass.

Ramaswamy, V., and S. M. Freidenreich (1991), Solar radiative line-by-line determination of water vapor absorption and water cloud extinction in inhomogeneous atmospheres, *J. Geophys. Res.*, *96*, 9133–9157.

Ray, P. S. (1972), Broadband Complex Refractive Indices of Ice and Water, *Appl. Opt.*, *11*(8), 1836–1844.

Ricchiazzi, P., and S. R. Yang, et al. (1998), SBDART: A research and teaching software tool for plane-parallel radiative transfer in the Earth's atmosphere, *Bull. Am. Meteorol. Soc.*, *79*(10), 2101–2114.

Rothman, L. S., et al. (1992), The HITRAN molecular database—Editions of 1991 and 1992, *J. Quant. Spectrosc. Radiat. Transfer*, *48*, 469–507.

Rothman, L. S., et al. (2003), The HITRAN molecular spectroscopic database: Edition of 2000 including updates through 2001, *J. Quant. Spectrosc. Radiat. Transfer*, *82*, 5–44.

Scott, N. A. (1974), A direct method of computation of the transmission function of an inhomogeneous gaseous medium-I: Description of the method, *J. Quant. Spectros. Radiat. Transfer*, *14*, 691–704.

Segelstein, D. (1981), The complex refractive index of water, M.S. thesis, Univ. of Missouri, Kansas City.

Stamnes, K., S. C. Tsay, W. Wiscombe, and K. Jayaweera (1988), Numerically stable algorithm for discrete-ordinate-method radiative transfer in multiple scattering and emitting layered media, *Appl. Opt.*, *27*, 2502–2509.

Stephens, G. L. (1984), The parameterization of radiation for numerical weather prediction and climate models, *Mon. Weather Rev.*, *112*, 826–867.

Toon, O. B., C. P. Mckay, and T. P. Ackerman (1989), Rapid calculation of radiative heating rates and photodissociation rates in inhomogeneous multiple scattering atmosphere, *J. Geophys. Res.*, *94*, 16,287–16,301.

Valero, F. P. J., R. D. Cess, and S. K. Pope (2004), Disagreements over cloud absorption, *Science*, *305*(5688), 1239.

van de Hulst, H. C. (1980), *Multiple Light Scattering: Tables, Formulas, and Applications*, vol. 1, Elsevier, New York.

Whitby, K. T. (1978), Physical characteristics of sulfur aerosols, *Atmos. Environ.*, *12*(1–3), 135–159.

Yang, S., P. Ricchiazzi, and C. Gautier (1999), Modified correlated k-distribution methods for remote sensing applications, *J. Quant. Spectrosc. Radiat. Transfer*, *64*, 585–608.

Wiscombe, W. J. (1977), The delta-M method: Rapid yet accurate radiative flux calculations for strongly asymmetric phase functions, *J. Atmos. Sci.*, *34*, 1408–1422.

Wiscombe, W. J., and J. W. Evans (1977), Exponential-sum fitting of radiative transmission functions, *J. Comput. Phys.*, *24*, 416–444.

Wiscombe, W. J., R. M. Welch, and W. D. Hall (1984), The effects of very large drops on cloud absorption: I. Parcel models, *J. Atmos. Sci.*, *41*, 1336–1355.

World Meteorological Organization (1986), Atmospheric ozone, Assessment of our understanding of the processes controlling its present distribution and change, *Rep. 16*, Global Ozone Res. and Monit. Project, Washington, D. C.

G. P. Anderson, Solar and Thermal Atmospheric Radiation, NOAA Climate Monitoring and Diagnostics Laboratory, 325 Broadway R/E/CG1, Boulder, CO 80303, USA.

A. Berk, Spectral Sciences Inc., Burlington, MA 01803, USA.

B. Bonnel, O. Boucher, and Y. Fouquart, Laboratoire d'Optique Atmospherique, F-59655 Villeneuve d'Ascq, France.

F.-L. Chang and Z. Li, Earth System Science Interdisciplinary Center, University of Maryland at College Park, 2207 Computer and Space Sciences Building, College Park, MD 20742, USA.

M.-D. Chou, Department of Atmospheric Sciences, National Taiwan University, Number 1, Section 4, Roosevelt Road, Taipei 106, Taiwan.

E. E. Clothiaux, Department of Meteorology, Pennsylvania State University, 503 Walker Building, University Park, PA 16802, USA.

D. Crisp, Jet Propulsion Laboratory, MS 180-404, 4800 Oak Grove Drive, Pasadena, CA 91109, USA.

P. Dubuisson, ELICO, Université du Littoral Cote d'Opale, 32 Avenue Foch, F-62930 Wimereux, France.

B. A. Fomin, Kurchatov Institute, Kurchatov sq. 1, 123182, Moscow, Russia.

S. Freidenreich and V. Ramaswamy, NOAA Geophysical Fluid Dynamics Laboratory, P.O. 308, Princeton University, Princeton, NJ 08542, USA.

C. Gautier, P. Ricchiazzi, and Y. Shiren, Institute for Computational Earth System Science, University of California, Santa Barbara, Ellison Hall Room 6804, Santa Barbara, CA 93106, USA.

R. N. Halthore, Remote Sensing Division, Naval Research Laboratory, 4555 Overlook Avenue, SW, Washington, D. C. 20375, USA. (halthore@nrl.navy.mil)

S. Kato, Center for Atmospheric Sciences, Mail Stop 420, NASA Langley Research Center, Hampton, VA 23681-2199, USA.

I. Laszlo, NOAA National Environmental Satellite Data and Information Service, 5200 Auth Road, Camp Springs, MD 20746-4304, USA.

J. H. Mather, Pacific Northwest National Laboratory, P.O. Box 999, MSIN K9-24, Richland, WA 99352, USA.

A. Plana-Fattori, Departamento de Ciencias Atmosfericas, Instituto Astronomico e Geofisico, Universidade de Sao Paulo, Rua do Matao 1226, CEP 05508-900, Sao Paulo, Brazil.

S. E. Schwartz, Atmospheric Sciences Division, Brookhaven National Laboratory, Upton, NY 11794, USA.

A. Trishchenko, Canada Centre for Remote Sensing, Natural Resources Canada, 588 Booth Street, Ottawa, Ontario, K1A 0Y7, Canada.

W. Wiscombe, Climate and Radiation Branch, Laboratory for Atmospheres, Code 913, NASA Goddard Space Flight Center, Greenbelt, MD 20771, USA.